Republic of Iraq

Ministry of Higher Education

and Scientific Research

University of Babylon

College of Engineering

Department of Electrical Engineering

Implementation of Low Cost Electronic Fabrication System

A Thesis

Submitted to the Department of Electrical Engineering / College of Engineering / University of Babylon in Partial Fulfillment of the Requirements for the Degree of Master in Engineering/ Electrical Engineering/ Electronic.

By

Ahmed Mohsin Naser Hussein

Supervised by

Asst. Prof. Dr. Haider Al-Mumen

2023 A.D. 1445 A.H.

بِسْمِ اللَّـهِ الرَّحْمَـٰنِ الرَّحِيمِ

(يَرْفَعِ اللَّهُ الَّذِينَ آمَنـــــُوا مِنكُمْ وَالَّذِينَ أُوتُـــــوا الْعِلْمَ دَرَجَاتٍ﴾

صدق الله العظيم

سورة المجادلة: 11

Supervisors Certification

I certify that this thesis (Implementation of Low Cost Electronic Fabrication System) and submitted by the student (Ahmed Mohsin Naser Hussein**)** under my supervision at the Electrical Engineering Department, College of Engineering at the University of Babylon, in partial fulfilment of the requirements for the degree of Master of Science in Electrical Engineering/Electronic.

Signature:
Supervisor: Asst. Prof. Dr. Haider Al-Mumen
Date: / / 2023

In view of the available recommendation, we forward this thesis for debate by the examining committee.

Signature:
Head of the Department: Prof. Dr. Qais Kareem Omran
Date: / / 2023

Examining committee certificate

We certify that we have read this thesis entitled (Implementation of Low Cost Electronic Fabrication System) and as an examining committee, examined the student (Ahmed Mohsin Naser Hussein) in its content and that in our opinion it meets standard of a thesis for the degree of master in engineering/electrical engineering /Electronic.

Signature:
Prof. Dr: Osama Al-Thahab
Chairman
Date: / / 2023

Signature:
prof. Dr. Mohmmed Nadim
Member
Date: / / 2023

Signature:
Asst. Prof. Dr. Hilal Hussein
Member
Date: / / 2023

Signature:
Asst. Prof. Dr. Haider Al-Mumen
Supervisor
Date: / / 2023

Approval of Head of Department
Signature:
Prof. Dr. Qais Kareem Omran
Date: / / 2023

Approval of Dean of Collage
Signature:
Prof. Dr. Laith Ali Abdul Rahaim
Date: / / 2023

Acknowledgements

Thanks be to God for the insight that inspired me, and praise be to Him for the blessings He has bestowed upon me, and to Him is the credit for achieving what I aspire to in this research. Praise be to God, who by His praise opens every book and by His remembrance every speech is issued, and by His praise, the people of blessings enjoy the abode of reward. It gives me great pleasure to extend my thanks and gratitude to (**Asst. Prof. Dr. Haider Al- Mumen)** who provided me with the information I needed for my research and for the great efforts he made for me since he proposed the subject of the research and his continuous supervision, and for his advice that helped me a lot in overcoming the difficulties I faced, calling from God success and brilliance in the scientific career. I would like to extend my thanks and gratitude to the Deanship of the College of Engineering and the Presidency of the Electrical Engineering Department for the facilities and administrative procedures they provided me, which effectively contributed to the completion of the requirements of this research.

Researcher

Ahmed Mohsen Naser

Dedication

To my kind father. who taught me how to stand firmly above the earth, my role model, and my ideal in life; He is the one who taught me how to live with dignity and honour. to my dead mother. I wish you mercy and forgiveness. To my brothers. Those who support me and share my sorrows before my joys. I dedicate to you the summary of my scientific effort.

Abstract

This thesis investigates the method of Implementation of Low Cost Electronic Fabrication System as a means of developing thin films of copper and aluminum on glass, silicon and plastic substrates .in a try to establish the experimentally created film thickness, ways for computing thickness are also explored and look into. A full discussion of the design and operation of the vacuum apparatus used to create the copper and aluminum films. were evolution is given as well as the next enhancement that could be made. Atomic Force Microscopy (AFM) was used for crystallography and morphology investigation of atomic forces microscopic. It shows the roughness increased with increasing thickness. The purpose of evaporation of more than one material, examination by atomic force microscopy, for more than one material and on more than one substrate is to ensure the efficiency of the device in the deposition of thin films, to know the required high currents and to know the high vacuum pressures. No deposition getting when current below 135 A. No deposition occurs when deposition time is below 35 minutes. Through the results obtained and through comparisons made with other devices, the device used gives similar results with a higher current, lower pressure, a less complex cooling system, and a larger power supply unit. this study also focuses on refining the photolithography step to increase alignment and critical dimension implementation, which is a quality parameter for semiconductor devices. The anticipated performance of the optimal option is found to be close to the model's expected limit of improvement. A photoresist layer is applied to the material to be patterned. Depending on whether positive or negative photoresist that used, the exposed or unexposed photoresist components were removed during the resist development process. Mask design is created, it can produce various mask designs in micro level scale by AutoCAD program. The

resulting PDF file mask design is printed as a positive film. in this experiment, uniform layer glass is used as a substrate with a length of 2.5 cm and width of 2.5 cm with a thickness 0.2 cm. Various elements, such as contamination, adhesion, exposure rate, sensitivity, and exposure source, affect photoresist performance.

Table of contents

List of Figures

List of abbreviations

Abbreviation	Definition
AFM	atomic forces microscopic
DI water	Deionized water
Fe2C13	Ferric Chloride
Kn	Knudsen number
ROI	Return on investment

List of Symbol

Symbol	Definition
α	evaporation coefficient
d	molecule's diameter
k_B	Boltzmann constant
ι	Mean free path
t	the thickness of the deposit where the vapors generally fall
$t_\circ$	The thickness of the deposit at a distance χ from this point

List of Tables

Publication

1. Ahmed Mohsen Naser and Haider Al-Mumen; "Low-Cost Thermal Evaporation Instruments, Design, Implementation, And Evaluation" 7th International Conference on Engineering Sciences (ICES) 2023. accepted for Publication. 24/10/2023.

2. Ahmed Mohsen Naser, Haider Al-Mumen; "Simple and Low-Cost Rapid Prototyping Fabrication by Using a Photolithography". Journal of University of Babylon for Engineering Sciences (JUBES). (accepted for Publication).286. 15/10/2023

CHAPTER ONE

Introduction

1.1 Overview

The fabrication technique is usually used for the fabrication of integrated circuits, optical devices and microelectromechanical systems [1]. Electronics Microfabrication technology has gotten a lot of interest in the last decade because of its capacity to downsize electronics utilizing highly integrated micro-devices [2]. Conventional Electronics production procedures, on the other hand, utilize the same semiconductor manufacturing equipment used to manufacture large- and small-scale integrated circuits and typically involve tens of processes. As a result, electronic fabrication necessitates a big capital investment and has high production costs, which generate issues [3]. Metals and nonmetals are deposited through thermal evaporation, Aluminum, chromium, gold, copper, and many other elements [4]. Multi-component deposition is a more complex application that can be done by carefully controlling the temperature of individual crucibles [5]. Metallic contact layers for thin-film electronics can be deposited using thermal evaporation, such as OLEDs, solar cells, and thin-film transistors. This method is also useful for depositing thick indium layers for wafer bonding [6].

1.2 Applications of Low-Cost Electronics Fabrication

The main purposes of PVD coatings are to increase hardness, wear resistance, and oxidation resistance. As a result, these coatings are employed in a variety of applications, including [7]:

- Dielectric and metal films
- Rotary shadowing for carbon & metals
- Small-scale manufacturing
- Forensic analysis
- Failure analysis
- Quality assurance
- Jewelry
- Extracts in liquid, soft, and dry form.
- In the concentration of blood plasma & serum.
- Water and solvent removal from fermentation broths.
- Penicillin and associated product concentration

1.3 Literature Survey

This section presents a scientific review of current research on Implementation of Low Cost Electronic Fabrication System.

In 2021, Divakar, A. Serja et al. [8], Design of low-cost UV exposure system which can be used for both high resolution and low-resolution photolithography. In first part, we present the study of irradiance distribution patterns of different UV LED arrangements, use uniformity as a criterion for selecting the arrangement that gives the best illumination uniformity in largest area. The maximum, minimum and average exposure energy and uniformity have been presented. Using these results, an optimal system design present for UV photolithography. The novelty of this work is simulating the UV exposure system for different parameters for making an optimal choice for a versatile system, different uniformity for different resolution to save power and have better control.

In 2023, D. Abdelmonem, S. Aly, M. Abdel-Rahman, and E. Shaaban et al. [9], 1 m thick Cadmium Telluride (CdTe) coatings on glass substrate were created using A Denton Vacuum Coating Unit thermal evaporator (DV 502 A) and vacuum of around 10^{-6} bar was used (at temperature about 150 C). The doped films were annealed in vacuum for 60 minutes at various temperatures (RT, 100, 200, 300, 400, and 500 C). Cu was present in an average concentration of 10±2% throughout all treated films, which was essentially constant. The conceivable transition in these as-deposited and as-treated films is found to permit a direct transition with a band gap reduction from 1.50 at room temperature to 1.29 at 300 C with a rise in temperature.

In 2023, Maryam Gholizadeh Arashti, Ebrahim Hasani et al. [10], The thin films with the thickness of 100 nm were fabricated at 150 °C under the pressure of 2×10^{-5} mbar using the thermal evaporation method. The x-ray diffraction (XRD) results showed that all grown CdS films had cubic crystal structures with the preferred orientation (111) and a crystallite size between 11.72 nm and 14.84 nm

In 2023, Nashreen F. Patel , Sanjay A. Bhakhar et al. [11], demonstrate the fabrication of large area photodetector based on thermally evaporated Bi_2Se_3 thin film for visible light detection. This thin film has thickness of 5000 Å and highly crystalline structure with (006) prominent orientation. Photodetector based on Bi_2Se_3 thin film shows excellent light sensitivity in broad spectral range from 485 to 670 nm.

In 2023, Hiba M. Ali, I. Khudayer et al. [12] Silver selenide telluride Semiconducting (Ag2Se0.8Te0.2) thin films were by thermal evaporation at RT with thickness350 nm at annealing temperatures (300, 348, 398, and 448) °K for 1 hour on glass substrates using X-ray diffraction. AFM techniques were used to

analyze the surface morphology of the Ag2SeTe films, and the results showed that the values for average diameter, surface roughness, and grain size mutation increased with annealing temperature (116.36-171.02) nm.

In 2023, I. Guler, M. Isik N. Gasanly et al. [13]. Thin film structure of $Tl_2In_2S_3Se$ $[(TlInS_2)_{0.75}(TlInSe_2)_{0.25}]$ material with layered structure was grown by thermal evaporation method and using Edward C that high cost and complex. The structural, morphological, and optical properties of the deposited thin films were examined. Atomic force microscopy (AFM) techniques were used to get information about structural and morphological properties of the thin films. XRD pattern presented well-defined peaks associated with monoclinic crystalline structure.

In 2023, D. Dastan, Ke shan, Azadeh Jafari, Tomasz Marszalek et al. [14]. NiO thin films are prepared on Ni foil using thermal evaporation method and the effect of deposition conditions on structural, morphological and H_2S gas sensing properties of NiO thin films is investigated. Structural analysis of the NiO films are conducted by means of X-ray diffraction (XRD). it is shown that the crystallite size and the size of homogeneous nanoclusters on the surface of the films increase after increasing oxidation temperature

In 2023, Biswal, Sameer Ranjan et al. [15], γ CuI thin films are grown on silicon substrates using a horizontal thermal evaporation system and using Edward C that high cost and complex, and the effect of gas flow on CuI thin film properties is thoroughly discussed. The X-ray diffraction (XRD) study confirms its polycrystalline nature and the γ phase of Cu I.

In 2023, Hiba M. Ali, I. Khudayer et al. [16], This survey investigates the thermal evaporation of Ag2Se on glass substrates at various thermal annealing

temperatures (300, 348, 398, and 448) °K. To ascertain the effect of annealing temperature on the structural, surface morphology, and optical properties of Ag2Se films, investigations and research were carried out. The Ag2Se films surface morphology was examined by AFM techniques; the investigation gave average diameter, surface roughness, and grain size mutation values with increasing annealing temperature (75.74 nm–96.36 nm).

In 2023, V. Travkin, Sachkov, Koptyaev et al. [17], attempt to systematically introduce five synthetic etioporphyrin (EtioP) complexes with copper and nickel into archetypal thin-film photovoltaic cells fabricated entirely by vacuum thermal evaporation. It is shown that EtioPs act as effective donors in a planar heterojunction, where another porphyrinoid molecule, hexachloro-sub phthalocyanine boron chloride Cl_6SubPc, is used as an acceptor.

In 2023, E.M. El-Zaidia, R. Bousbih, A. Darwish et al. [18], Thermal evaporation was used to grow films of the compound boron sub phthalocyanine chloride (B-sub PcCl) on glass substrates. X-ray diffraction was utilized to investigate the structural nature of B-Sub PcCl evaporated thin films. The investigation of the film's structure exhibits the amorphous structure of the present films. Atomic force microscopy was used to examine the surface topography and grain size. B-sub PcCl films are constructed of spherical nanoparticles.

In 2023, Zainab Qassim Mohamed; Abdelaziz O. Mousa Al-Ogaili; Khalid Hanen Abbas et al. [19]. The films we are characterized morphologically by atomic force microscopy and optical properties are examined also by UV-Visible spectrometer, cupreous oxide (Cu_2O) nanofilms which synthesized by thermal evaporation technique with pressure up to 10^{-7}mbar, with thickness (75) nm. The surface morphological properties of Cu_2O films were examined via an atomic force

microscope (AFM). The root mean square, average roughness, number of grains on the surface, and average diameter are studied from atomic force microscopy.

In 2023, M. Bathaei, R. Singh, H.Mirzajani, E. Istif, L. Beker et al. [20] a batch fabrication-compatible photolithography-based microfabrication approach for biodegradable and highly miniaturized essential sensor components is presented on flexible and stretchable substrates. Up to 1600 devices are fabricated within a 1 cm^2 footprint and then the functionality of various biodegradable passive electrical components, mechanical sensors, and chemical sensors is demonstrated on flexible and stretchable substrates. The results are highly repeatable and consistent, proving the proposed method's high device yield and high-density potential. This simple, innovative, and robust fabrication recipe allows complete freedom over the applicability of various biodegradable materials with different properties toward the unique application of interests.

In 2023, Woo-Kyung Lee , E. Whitener et al. [21] demonstrate an approach where the photolithography is performed and developed on a planar surface and the completed photo pattern is then transferred to an arbitrary substrate. We achieve this transfer using two different release layers: a graphene-based layer which can produce closed windows, and a gelatin-based layer which produces open windows. In the gelatin case, pattern gold features directly on a curved substrate with at least 2-μm fidelity.

1-4 Problem Statement

- The high cost of the thermal evaporator
- The difficulty of maintaining its complex parts.
- Lack of availability in local markets

1.5 Thesis Objectives

The main objective of this thesis is:

- ❖ Make Low-Cost Electronics Fabrication System by Production of thin films at low costs. These thin films can be used in the electronics industry.
- ❖ After manufacturing thin films by thermal evaporation, the photolithography process is carried out to produce the appropriate pattern at a low cost as well.

1.5 Thesis Outline

The thesis is divided into five chapters.

Chapter One

which comprise a general introduction to Implementation of Low Cost Electronic Fabrication System, a thesis proposal, and a literature evaluation of existing studies in the subject of Low-Cost Electronics Fabrication.

Chapter Two presents an overview of the Low-Cost Electronics Fabrication technology that has been used in this industry and how it has in recent years, it has grown.

Chapter Three Describes the electronic fabrication system and all of its specifics, comprising system prerequisites and implementation tools.

Chapter Four includes a result of the electronic Fabrication system as well as a discussion and analysis of the results acquired via this study.

Chapter Five Contains the most essential work conclusions and recommendations for further work.

Chapter Two
Theoretical Concepts

2.1 Thermal Evaporation

Fabrication is commonly used to made integrated circuits, Optoelectronic devices, and Microelectromechanical systems (MEMS). The cost and availability of particular devices are constraints for this type of fabrication. Fabrication technology is gaining popularity because of its potential to shrink circuits utilizing highly integrated micro-devices [22]. Conventional Electronics fabrication procedures, on the other hand, use the same semiconductor manufacturing technologies that used to manufacture large- and small-scale integrated circuits and typically require tens of processes. As a result, electronic fabrication necessitates a big capital investment and has high production costs, which generate issues. The cost of fabricating electronic gadgets is high [23]. Thermal evaporation deposits in both materials, including aluminum, copper, and others. Implementation of Low Cost Electronic Fabrication System is commonly hard. Given the complexity, it's logical that the first films were made with flashing metal wire. Flashing, also known as flash evaporation, happens when a high current is passed across a wire, causing it to sublimate. Thermal evaporation is a common method of Physical vacuum deposition that employs a resistive heat source to produce a thin film by evaporating a solid material in a vacuum environment. In a high vacuum chamber, the substance is heated till vapor pressure is created. The evaporated substance, or vapor stream, is carried by heat energy through the vacuum chamber and coats the substrate [24]. Metals and nonmetals, such as aluminum, chromium, gold, copper, indium, and many

more, are deposited via the thermal evaporation system with Substrate heating. This thin film deposition technology is most commonly employed for electrical contact applications, where single metals such as copper are deposited. PVD is a deposition method that deposits thin films onto a substrate by condensing a vaporized form of the desired film material [25]. The solid coating substance is evaporated by heat in the PVD process. Simultaneously, gas and metal vapor and is deposited as a thin film with a highly adherent coating on the substrate. The substrate is the object to be coated and can be anything from semiconductor wafers to solar cells to optical components and many more possibilities [26]. It is typically near the bottom of the chamber, often in the form of an upright crucible. The vapor rises above this bottom source, and the substrates are kept inverted in the chamber's top fittings. The coated surfaces are thus oriented downward toward the hot source material to get their coating. Thermal Evaporation system design allow for the adjustment of a number of parameters, allowing process engineers to get good results for variables such as thickness, uniformity, adhesion strength, grain structure, and so on. sometimes known as a filament [27]. ones of these resistive evaporation filaments have diverse physical forms, including ones that are known as "boats". The filament source provides low voltage safety, but it demands a very high current, often several tens’ amps. Thin Film Evaporation systems can provide reasonably high deposition rates, real-time rate and thickness control, and (with appropriate physical construction) effective evaporate stream directional control for lift-off processing to generate directly patterned coatings [28].

2.2 Advantages of Thermal Evaporation

- The capacity to utilize nearly any inorganic and certain organic coating materials on a wide variety of substrates and surfaces with a variety of finishes.
- Less harmful to the environment than standard coating methods like as electroplating and painting.
- A given film can be deposited using more than one process.
- Highest purity (Good for Schottky contacts) due to low pressures.
- Excellent adherence

The most fundamental quality of PVD procedures is that vapors are transported by physical mechanisms transfer from the source to the substrate. This is accomplished by performing the deposition effectively in such a way that the free path of the molecules in the ambient gas is so long that it surpasses the dimensions of the deposition chamber and the source-to-substrate distance. Because of the low pressure, molecular beams transfer the material from the source to the substrate [29]. Thermal evaporation can produce vapor species from solid materials. The process of deposition in the former case is referred to as vacuum evaporation. In pure PVD techniques, the deposits are formed from atomic or molecular units, simply by the physical process of condensation. A chemical reaction between various gases is purposely induced at the substrate in some situations. As a result, both vapor movement and deposition occur via physical processes in PVD procedures.

2.3 Vacuum Technology

All procedures and physical measurements are conducted at air pressures lower than typical. A procedure or physical measurement is typically done in a vacuum for one of the reasons listed below:

1. Remove any elements of the atmosphere that could cause a chemical reaction or physical during the evaporation.

2. Disrupt a balance situation that exists under regular room conditions.

3. Increase the distance between particles before they collide, allowing particles in a process to go forward without interfering with one another.

4. Reduce the number of molecule hits per second, lowering the likelihood of contamination of vacuum-prepared surfaces (helpful in clean-surface research). A limiting parameter for the maximum permitted pressure can be defined for any vacuum process. Reasons 1 and 2 can represent the number of molecules per unit volume, Reason 3 can be the mean free path, and Reason 4 can be the time necessary to build a monolayer. many procedures performed in a vacuum produced either greater results or outcomes that were previously unreachable with normal atmospheric conditions [30]. The ratio of the molecular mean free path length to a typical physical length scale is defined as the Knudsen number (Kn). If the Knudsen number approaches or exceeds one, the mean free path of a molecule is comparable to the length scale of the problem. The mean free path is calculated using eq (2.1):

$$\iota = \frac{0.00007}{P\ (in\ atm)} \quad \text{in (m)} \qquad (2.1)$$

where

P the pressure.

lowering the vacuum's base pressure will make the particles picked up as they travel towards the substrate to be deposited. The loading and unloading of samples are achieved through a set of manual operations, while the deposition of material can either be performed automatically or manually [31]. The system is capable of deposition on substrates of many sizes, from small pieces up to a 4" substrate. Even a few nanometers of this natural barrier layer can hinder correct adhesion or influence the conductivity of the layer stack, both of which are crucial for semiconductors [32]. The rate of vapor condensation is affected by the geometry of the source, its position relative to the substrate, and the condensation coefficient. The deposit distribution is defined by:

$$t/t_{\circ} = 1/\left[1 + \left(\frac{\chi}{h}\right)^{2}\right]^{1.5} \quad (2.2)$$

were

t is the thickness of the deposit where the vapors generally fall and

$t_{\circ}$ is the thickness of the deposit at a distance χ from this point.

h is the distance between substrate and point source.

The vapor pressure should be obtained by adjusting the source temperature.

2.4 Thin Film

A thin film is a layer of material whose thickness ranges from nanometers to several micro meters. Mainly used in semiconductor devices, semiconductor electronics. The common application of thin film is hushed mirrors, hard coating on cutting tools, and for both energy generation (thin film solar cells) and storage (thin film batteries). In addition to their applied interest, thin films play an important role in the development and study of materials with new and unique properties [33]. Thin film deposition by Chemical, physical and electrochemical

general methods used for the deposition of various materials was tested for preparation. The key feature of thin film technology is that "self-organizing" structure growth occurs via an atom-by-atom addition process at temperatures far from thermodynamic equilibrium, which allowing for the controlled creation of metastable phases artificial structures such as multilayers and nanocomposites. Deposition of a trace quantity of active additive is another way to regulate structure evolution and structure. Thin film applications have evolved significantly over time [34]. Thin film deposition can improve the adaptability and utility of a material by boosting surface attributes such as wear, fatigue, corrosion, hardness, and other surface-related phenomena. These applications can be classified into the following generic categories:

- Display and electronic components. it has greatly improved compound conductor films for semiconductors, dielectric and insulating materials, and metal refractory silicide conductors. Electronic displays necessitate the use of conductive and transparent films, luminous or fluorescent films, as well as dielectric and insulating layers [35].
- Biomedical and solid surface coating. Component tribology resistance and corrosion performance can be increased by coating the component's surface with thin film coatings of carbides, silicide’s, nitrides, and borides, in that order. These coatings are employed in tool manufacturing, which involves sliding friction, such as bearings and machine parts.

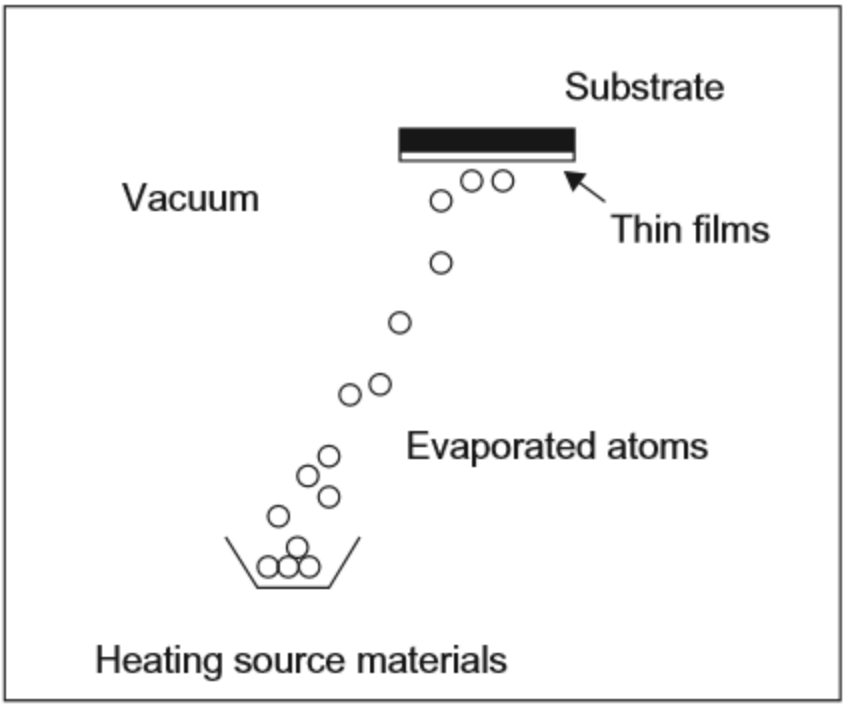

Fig (2.1) A typical vacuum thin film deposition apparatus [27].

Thin films are formed by depositing atoms of a substance on a substrate, Fig (2.1) show a typical vacuum thin film deposition apparatus. A typical thin layer growth technique on a substrate using material atom deposition [36]. The deposition procedure controls the characteristics of thin films. There are some things that must be taken into account as they are included in the core of thin films.

2.4.1 Film Thickness

This refers to the thin film coating's thickness. To ensure performance, your thin film coating must be within the proper thickness parameters for your individual application. Some applications, for example, necessitate a very fine, accurate coating to allow for the proper degree of light transmission. Other applications necessitate a thin layer coating for durability and protection; thus, they can be a

little thicker and less accurate. Thickness has significant consequences for next-generation products.

2.4.2 Film Uniformity

One of the most significant features in all applications and coatings is uniformity. If the thickness distribution is uneven, the overall durability and performance of the film may suffer. Some substrates have a more complicated topography, with bumps and vias, but the thickness must also be uniform over the surface [37].

2.4.3 Grain size

Individual crystallites or particles make the solid metals, and the size of these particles is referred to as grain size. Many other properties of the metal, most notably its density, are determined the grain size. High energy and higher particle migration result in smaller grain sizes, while low energy and lesser migration result in bigger grain sizes. Density is inversely proportional to grain size, hence for high-density applications, you want a coating with more particle movement and a smaller grain size. You can improve the wear resistance and strength of the thin film by changing the grain size and density [38].

2.4.4 Throughput

The number of substrates that your thin film can coat per hour is referred to as throughput. It's one of the most fundamental metrics of system efficiency, and it has a substantial impact on your ROI and cost of ownership. It is vital for high-volume applications to have a system that can meet high throughput needs. Lower-volume applications may not necessitate such a high throughput.

2.4.5 Adhesion

Adhesion determines the stability of a thin layer. If a coating has strong adhesion, it will adhere tightly to the wafer or substrate, increasing production yield and overall reliability. Because of increased gadget performance and a longer lifetime, good adhesion contributes to a better user experience. Moisture and hydrocarbons can both be detrimental to adhesion, so a pre-cleaning treatment to remove such molecules may be required [39]. To improve metallization adhesion, you must also prevent oxidation between the adhesion and conduction layers. This can be accomplished by covering numerous layers while maintaining the vacuum.

2.5 Patterning

The decoration is the backbone of the transistor size Reduced to what it is today, making modern electronic devices increasingly affordable. Thus, patterning is also the driving force behind many developments in semiconductor manufacturing techniques [40]. Create a small interconnected three-dimensional structure of insulators, semiconductors and conductors Transitionally distort regions of semiconductors to form junctions P – n with other electrical components and there are three types of Patterning, Photolithography, Electron Beam Lithography, Nano Imprint Lithography. The most one is photolithography. The use of low cost Electronics Fabrication System offers advantages such as flexibility, so that the inception tens of years ago, the microelectronics sector has grown dramatically. Improvements in the fabrication processes have resulted in a constant increase in the complexity of microcircuits while lowering the cost to the customer [41]. The switching speed and power consumption of individual circuit elements are enhanced by lowering their size, switching speeds have risen by 100 times. during the previous several decades [42]. A good illustration of this impact is the halving of the cost of memory

devices per bit every two years. Lithography is the capacity to define detailed patterns on the surface of a glass wafer is a critical step in the creation of microcircuits. To address the demand for smaller geometry devices, optical lithography techniques have continually grown and improved [43]. One key advantage of optical lithography is that it is basically a parallel information system. transmission method, making it suitable for bulk copying of complicated designs. Photolithography is a technique that uses light exposures to pattern a layer of photoresist. A positive photoresist is one that gets more soluble upon exposure and dissolves the exposed portions [44]. Negative photoresist occurs when exposed parts of photoresist become less soluble and unexposed areas are eliminated during development. Photolithography is a process that transfers shapes from a template onto a surface using light and used in micromanufacturing applications [45]. Lithography is the printing method used in the semiconductor industry to mass-create chips like microprocessors and memory. The requirements of photolithography are high resolution, High photoresist Sensitivity, precision alignment, Precise Process Parameters control, and low defect density. lithography costs 50% of the cost of creating a modern chip (integrated circuit). To keep Moore's law continuing, more transistors are collected on a chip by making each transistor smaller; Lithography advancements must enable the printing of smaller features without materially raising the chip's cost. The Applications of Photolithography are Fine Screen and meshes, fuel cell components, sensors, pressure membranes, heat sinks, flexible heating elements, RF and Microwave circuit parts, semiconductor lead frames, metal gaskets and seals, electrical contacts and encoders. Fig (2.2) show diagram for Photolithography Process.

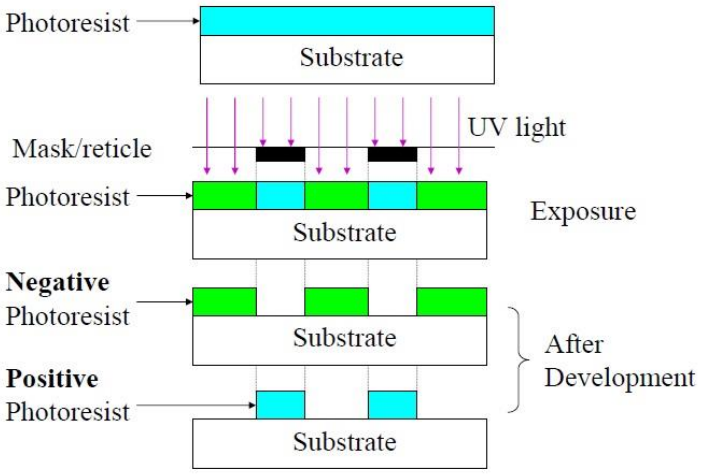

Fig (2.2) Diagram for Photolithography Process [44].

The photosensitive polymer can change their structure when exposed to radiation, and any changes in structure produce a change in properties which in turn producing an image on metal surface, photoresist protects the surface of metal from the action of the etching reagent. the applications of photoresist are spin coating, soft baking, convection, oven, vacuum oven, hot plate, microwave and IR lamps, exposure. for Positive Resist and After Exposure to the Proper Light Energy, the Polymers are Converted into a more Soluble state. For Negative Resist and After Exposure to the Proper Light Energy, the Polymers are Converted into a Less Soluble state. Fig (2.3) show a Positive and Negative Resist.

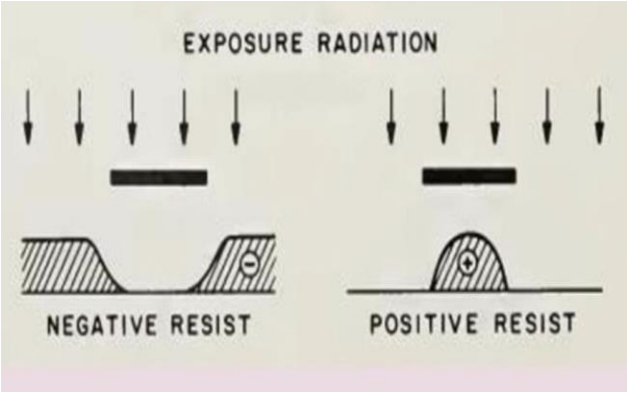

Fig (2.3) Positive and Negative Resist [41].

2-6 Atomic Force Microscope (AFM)

Through this technique, the topography of the surface can be identified, and the roughness and roughness rate are calculated, the used device was of the type (AA3000) equipped by Angstrom Advanced Inc. and the place is in (the University of Baghdad College of Science). Atomic force microscopy (AFM) is one of a larger family of the microscopes probe which including the scanner near-field optical microscope and the scanner tunneling microscope. the common factor between these microscopes they have a very accurate and sharp probe that interacts with the sample surface according to the attractive and repulsive forces to produce a high-resolution surface topography image. AFM device gives a three-dimensional image of the surface of the sample and can examine the solid and plastic materials, whether industrial or natural, and the environment of the sample is often air, and it may be a liquid and in a special case a vacuum. The images obtained from AFM do not depend on the usual methods (that is, by relying on reflections and aberrations) as in the case of electron and optical microscopy. AFM depends on the tactile method to give an image to the sample surface, so it can be said that the AFM is a blind microscope scanner. The image can be obtained from Surface topography, and it depend on the following mechanisms:

- First: The dependence of the strength of the interaction between the probe that ends with a fine tip and the sample surface is the driver of the tip, which is rapidly changing with the distance, as it changes between an attractive force when a tip is on the sample to a repulsive contact force when a tip approaches the surface of the sample.
- Second: the movement of the surface scanner that scans the sample with the x-y plane, either by the movement of the sample while the tip remains constant or vice versa.

- Third: the presence of a sensor that works with the Z axis, which is very fast, move the probe closer or away from the surface of the sample according to the topography of the surface so that the distance is constant between the tip and the surface of the sample.
- Fourth: converting the motion of the probe while scanning the horizontal and vertical by a very accurate sensor. The operator can specify the dimensions of the measurement in terms of width and height in the form of dark and gradient colors according to the heights of the sample surface, which results in the observed image. Figure (2-4) shows the main parts of the AFM.

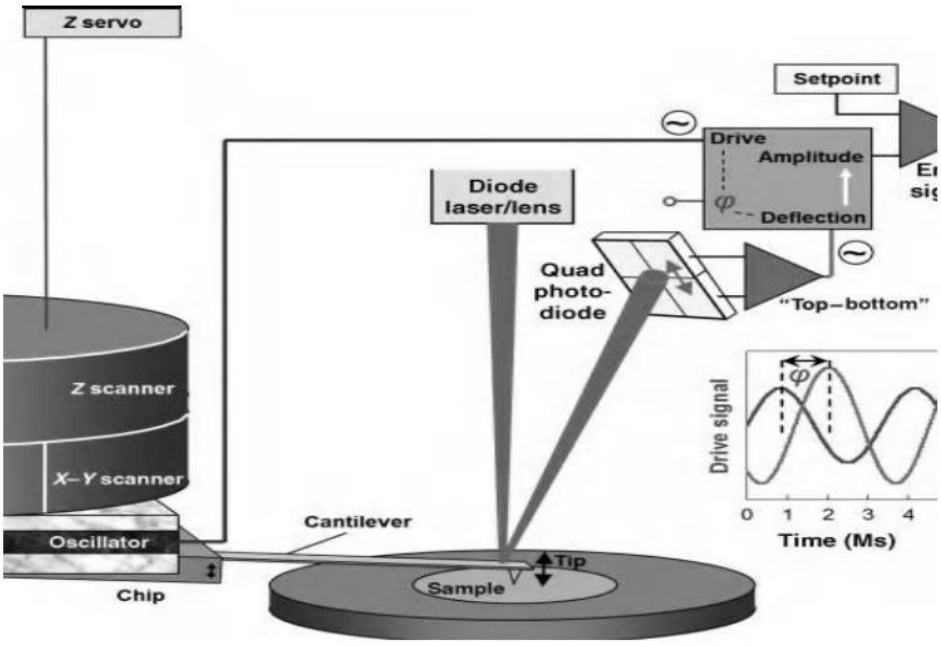

Fig (2-4) AFM.

Chapter Three

Proposed Evaporator System

3.1 Introduction

This chapter is divided into two main sections, the first part represents the design and operation of the physical thermal evaporation device, as well as examining the device by comparing the results with the results obtained from other devices. and the second part represents the photolithography process and compares these results with another result.

3.2 Thermal Evaporator Design.

Thermal evaporation is a deposition method in a high vacuum condition applying the electrical current to vaporize the source material and deposition on the substrate. The chamber's pressure, the boat's temperature, and the power supply current are the parameters that need to be controlled in this process. In this method, the source material will be placed in the boat or filament made of resistant metals (tantalum, Molybdenum, or tungsten). The electric current passing through the boat will make it hot and the source material will be vaporized and depositing a thin layer on the substrate. This part includes a detailed description of the device fabricated and the approved steps to prepare pure copper, and pure aluminum that we deposited Separately on the (glass, silicon, plastic) substrates and the factors affecting the preparation of the membranes. It also included a description of the devices used in mechanical, and electrical measurements. This work uses room-temperature evaporation. Fig (3.1) show the schematic diagram of thermal evaporator.

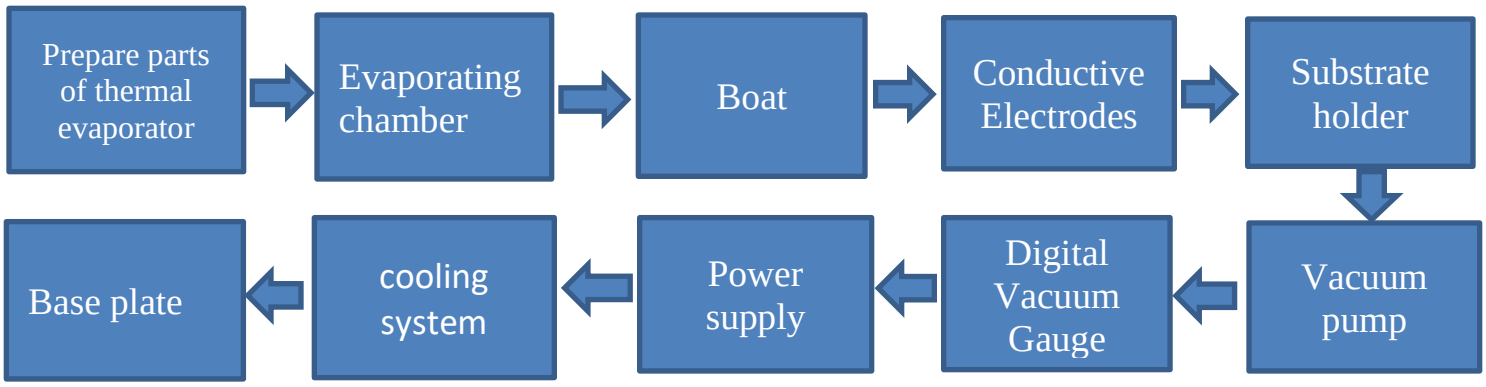

Fig (3.1) schematic diagram of thermal evaporator.

3.2.1 Evaporating chamber.

Evaporating chamber that is Pyrex cylindrical in shape with a height of about 25 cm and an inner diameter of about 15 cm, Thickness 0.7cm. It is made of glass that is resistant as shown in Figure (3-2).

Fig (3-2) Pyrex cylindrical chamber.

3.2.2 Substrate holder.

Substrate holder that is a stainless-steel disc with a diameter of 15 cm as shown in Fig (3-3), placed horizontally by four vertical screws fixed to the floor of the evaporating chamber, the distance of the substrate's holder can be controlled from the evaporation crucible. Any material might be used for the substrate.

Fig (3-3) Substrate holder.

3.2.3 Base plate.

The base plate should be designed with rails which allows at least 50% of the base plate to slide out of the chamber. The chamber should be designed considering an out-of-mass 40 kg that has a maximum size of 35 cm (length) X 30 cm (width) X 30 cm (height) and a heat load of less than 1200W. The chamber body should be mounted horizontally on a supporting structure.

3.2.4 Conductive Electrodes

Two conductive electrodes are made of copper being good conductivity as shown in Fig (3-4).

Fig (3-4) Two conductive copper electrodes.

3.2.5 Boat

The evaporation crucible is installed between the Two conductive electrodes and the other end as shown in Fig (3-5). Tungsten has the greatest melting point of all metals in pure form (3422°C), 4.5 cm long, 1 cm wide and 0.025 cm, it has Lowest vapor pressure and the highest tensile strength. Tungsten is also the pure metal with the lowest coefficient of thermal expansion Because of these qualities, tungsten is an excellent material for evaporation sources. It can alloy with some materials during evaporation, such as Al or Cu.

Fig (3-5) Tungsten boat.

3.2.6 Power supply.

Upgrading the heating element necessitated the search for a more suitable power source. The prior power supply could only deliver 20 and 40 amps, which was insufficient to adequately heat the new filament design. To accelerate electrons travelling through a conductor, Joule heating requires extreme currents and low voltages. A high current is similar to a big river of electrons flowing through the structure, and a high voltage is analogous to a strong accelerating force on the electrons.

Moving electrons "collide" with other atoms, transferring energy to the conductor's lattice structure. Increasing the number of "collisions" or the energy delivered by each collision causes a larger macroscopic temperature change.

AC Power Supply is shown in Fig (3-6) with Input Power with setting of 1320W, Input Voltage: 220V, Input Current: 6A, Frequency: 50 Hz, Output Voltage: 6V AC, Output Current: 200A, Shell Material: Metal case / Stainless steel base, Working Temperature: 0~50C°. The number of turns of the primary coil and the

secondary coil is 110 and 3 respectively. Ambient Humidity: 0~95% non-Condensation. A strong table with a length of 150 cm a width of 50 cm a height of a desk and a tolerance of 40 kg weight is needed. During the power supply investigation, we examined the equipment and searched for ways to enhance it. The high voltage feedthrough we were employing wasn't designed for heavy current utilization.

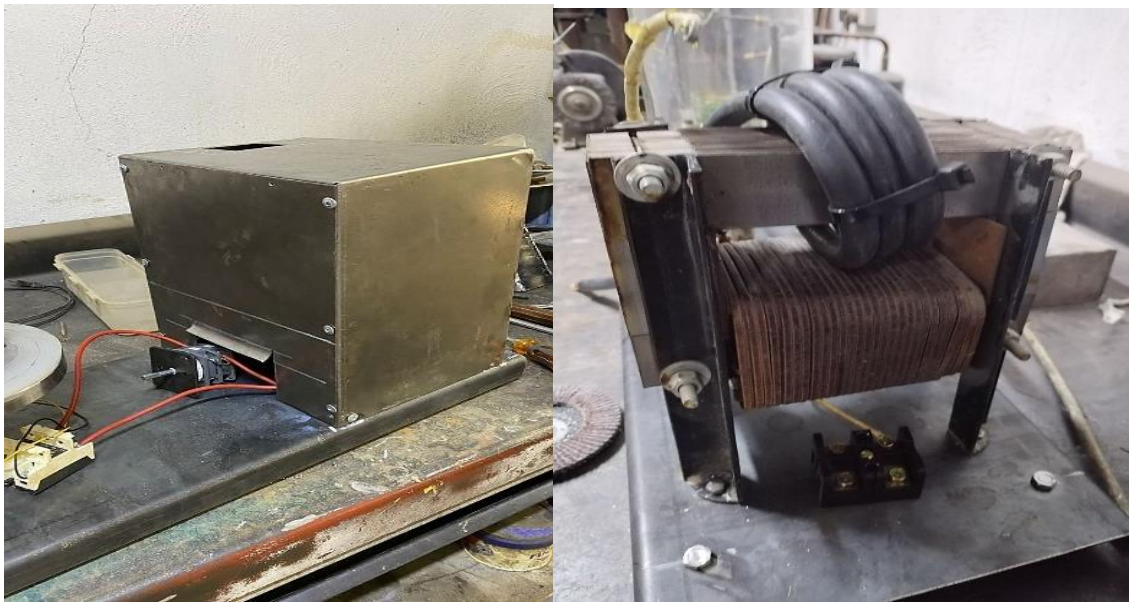

Fig (3-6) AC Power Supply in the stage of fabrication.

3.2.7 Cooling Fan

A ventilation fan was added to dissipate the heat as shown in Fig (3-7). The majority of power supply units have an intake fan that pulls in rather than expels air. This indicates that it is sucking in the air. The exhaust fan on the rear of the machine normally vents the air out of the casing. As a result, you should aim the intake fan at a source of cold air from outside the case.

Fig (3-7) Cooling fan.

3.2.8 Vacuum pump

Dual stage Vacuum pump VE 215 are used as shown in Fig (3-8) with depicted in table (3.1).

Table (3.1) Dual stage Vacuum pump VE 215 parameters.

oil capacity	180 mL
frequency	50 Hz
mass	7,5 kg
height	230 mm
width	124 mm
length	308 mm
Flow rate	2 CFM (50 Liters /minute)
optimum vacuum	0.3 Pa/25 microns
Pressure	10^{-6} bar
Inlet port	0.25
horsepower	0.25

Fig (3-8) pump VE 215.

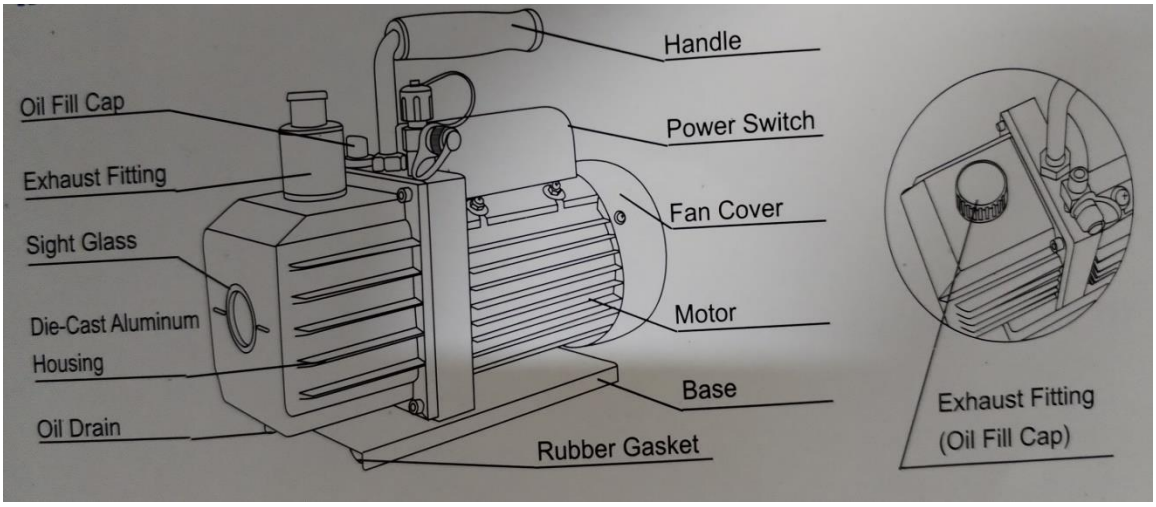

Fig (3-9) vacuum pump (VE 215)with markings on parts.

3.2.9 Digital Vacuum Gauge

Digital Vacuum Gauge with Model NO. VA-116A, is shown in Fig (3-10), This simple gauge ensures that all gases and Contamination have been eliminated from the chamber. The one-of-a-kind heat conductivity sensor adapts to temperature.

Replaceable, cleanable, plug-in sensor handles 450 psi positive pressure is used via a replaceable, cleanable, plug-in sensor. 3 Displays eight distinct vacuum units. Displays down to 10 microns, 0°C to 50°C, and the low battery indicated After 15 minutes, then the device shuts down automatically. weight with battery: 340 g. Measuring Range Low-pressure Gauge, Accuracy: 0.25, Radial Direction.

Fig (3-10) Digital Vacuum Gauge VA-116A.

3.2.10 Cooling System

The cooling System consists of a plastic bowl as shown in Fig (3-11).

Fig (3-11) Plastic bowl.

Plunger water pump with 220 v, frequency 50 Hz, 25-watt power and maximum suction of 1.8 m and a rated flow of 1000 Liter per Hour as shown in Fig (3-12).

Fig (3-12) plunger water pump

Finally, the Fig (3-13) shows Thermal evaporation device.

Fig (3-13) Thermal evaporation device

3.2.11 Substrate Preparing

We first Prepare the substrate that we deposited; the substrates used for depositing thin films by thermal evaporation are (glass, silicon, and plastic) substrates. the Substrates all of (2.5 × 2.5) cm2 area are with thickness 0.2 cm. The cleaning of the substrates is very important because it has a great effect on the properties of the thin films. The cleaning is as follows:

- ❖ put substrate in Acetone.
- ❖ put the substrate in the Isopropanol.
- ❖ put the substrate in the DI Water.
- ❖ dried in a thermal oven for 15 minutes or dry the slides by wiping them with soft paper later they can be ready to use in the deposition process.

3.2.12 Raw materials

Thin films of high purity (99.999) copper as shown in Fig (3-14) and supreme purity (99.999%) Aluminum as shown in Fig (3-15) Several times, they were employed as raw materials for evaporation

Fig (3-14) pure Copper granules.

Fig (3-15) pure wire aluminum.

3.2.13 Process of Evaporation

Fig (3.16) show the schematic diagram of thermal evaporation.

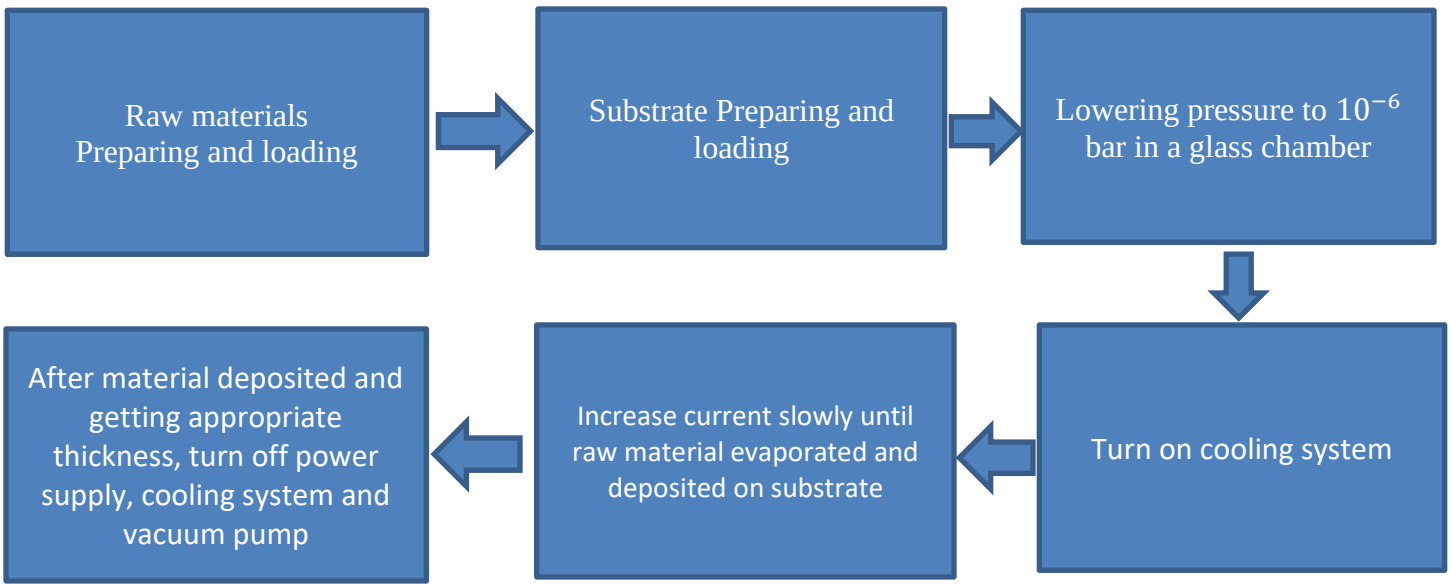

Fig (3.16) schematic diagram of thermal evaporation.

starts the roughing pump, places the system in Vent, and vents the chamber by turning the knob to "Vent". All the valves should be closed, after the chamber reaches atmospheric pressure 1 bar, the vacuum chamber will lift from the steel base plate. Loading the sample (2" wafers). The material was placed on a Tungsten boat with a small indentation in the center to serve as a point source, and a clean substrate slide was inserted inside the stand. Place the wafer facing down on top of the wafer holder, then replace the wafer holder inside the camper. A substrate is supported by a holder. The separation between the substrate and the boat is (10) cm. Thermal vacuum evaporation system with 10^{-6} bars placed on (glass, silicon, plastic) substrate, A substrate is mounted on a holder, and now the Tungsten coil is coated with copper and will be ready for thermal evaporation, The Pump setting opens up the roughing valve to evacuate the chamber, and the pumping line evacuates the vacuum chamber to a pressure of 10^{-6} bar via the pumping line. A vacuum gauge is used to measure pressure. A deposition pressure of 10−6 bar was achieved by utilizing a rotary pump in succession. When Pressure not pumping below 10^{-5} bar then clean the bottom of the glass chamber and the base plate again to ensure no leak from the glass chamber. And when No metal evaporates then change the Tungsten coil. There may be contaminations to the coil, After the vacuum chamber reached a high vacuum, a slow current was delivered to the electrodes to heat the substance, Rotate the ON / OFF switch clockwise on the right of the power supply. The AC power supply was also used independently to power the evaporator and increase electrode power to 135 Amps and measured in ammeter. The current flows through an isolated vacuum tight lead the charges will evaporate and the slide will be coated with melt. A material is evaporated from a metal boat heated by an electric current, the boat was heated indirectly by passing a current through the electrodes. Copper granules were evaporated from a tungsten crucible placed 10 cm away from the glass substrates. The deposited Cu & Al thin

films were heated Severally, and the increase of the thin films was prepared using thermal evaporation from a tungsten boat.

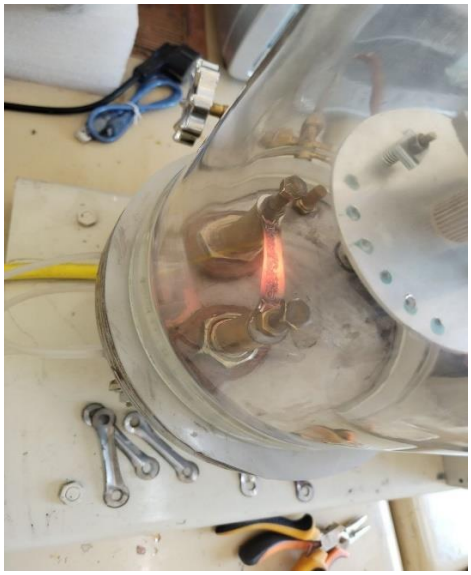

Fig (3-17) boat glow

The material was slowly outgassed before evaporation. The evaporated atoms transit vacuum to the surface of the substrates without collisions. For shutdown. Turn the current control back to 0 Amps to allow cooling. which is usually cooled by water. Wait 10 minutes for cooling before removing the wafers. The unload steps follow the same procedure as the load step. when wafers are removed and other apparatus are returned to the chamber, push down the pressure and turn the knob to the "PUMP" position. Hold the pressure down until the vacuum pulls down enough to hold it down and the chamber cannot be moved. When the coating is complete for the semester, turn the knob to "shut down"; To shut down your pump after use.

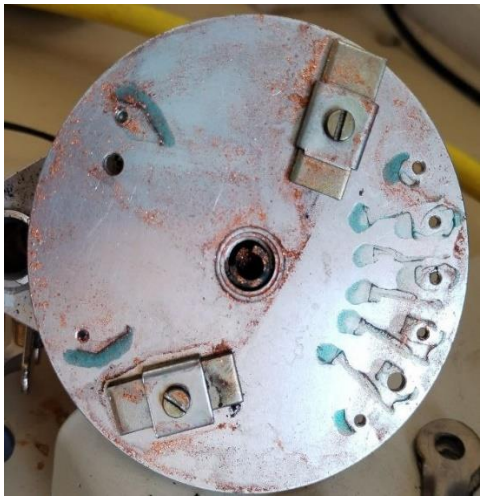

Fig (3-18) copper deposited on Substrate's holder.

3-3 Photolithography process.

Fig (3.18) shows schematic diagram of the photolithography process.

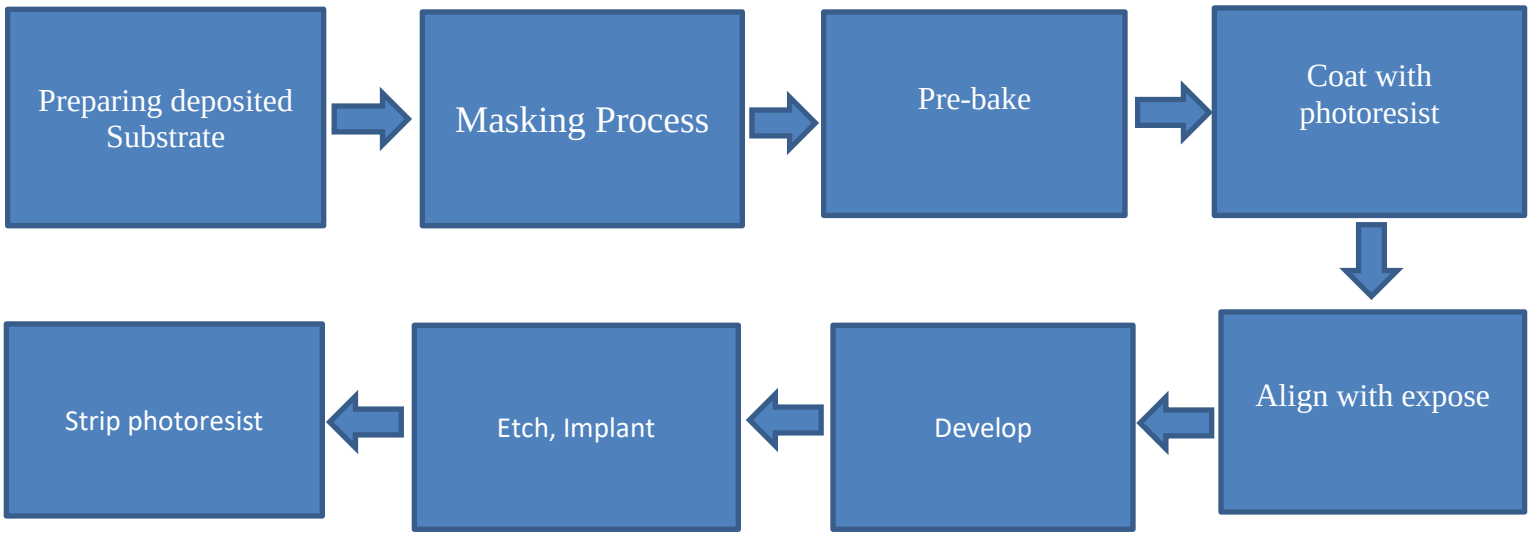

Fig (3.19) schematic diagram of the photolithography process.

The photolithography process can be involved the following steps:

3.3.1 Preparing substrate.

Photolithography begins with a substrate. The substrate is used as the foundation of the "film" on which a pattern will be created. Substrate choice depends on the ultimate operational goal of a given device. Glass can be used because transparency is desired. However, different substrates can require special attention, so processing must be optimized individually for each material this part includes a detailed description of the photolithography including the following process:

- Cutting into Require Size.
- Carefully Cleaned
- Photoresist Material Coating

In this experiment a Uniform Layer glass substrate is used, so that it deposited with (copper or aluminum) all of (2.5 × 2.5) cm^2 area is with a thickness 0.2 cm, Heat and pressure used to ensure good Adhesion, and prebake remove the dry photosensitive part from photoresist also hardens it.

3.3.2 Masking Process.

The mask, also known as a reticle, contains what you wish to print on the wafer opaque patterns on a transparent substrate, Making the photomask uses its own lithography process usually done by using beams of electrons to expose a resist, Pattern on the mask is defined by the chip design data, Mask is a Head Copy of Pattern and is essential parts of fabrication process. It is very important to miniaturize the submicron scale and be cost-effective in the making process. Typically, masks with glass plates are used for exposure. These are kept on the aligner by vacuum, and a wafer can be securely pressed onto the masks. Good

contact with a low gap between the mask and the wafer is critical during exposure to guarantee that the exposed features match the features on the mask and are not influenced by light diffraction. While chrome masks provide very small feature sizes and good contact exposure, but they are costly, and the process takes a long time to complete. Instead, emulsion masks on film sheets were used during the development of the fabrication procedures.

The advantages of emulsion masks include their inexpensive cost and short turnaround time. Because these masks are flexible, a different way of retaining them is required to reduce the gap between the masks and the wafer. Mask design is created in micro-level scale (μ m). The resulting PDF file mask design is printed as positive film as shown in Fig (3-20).

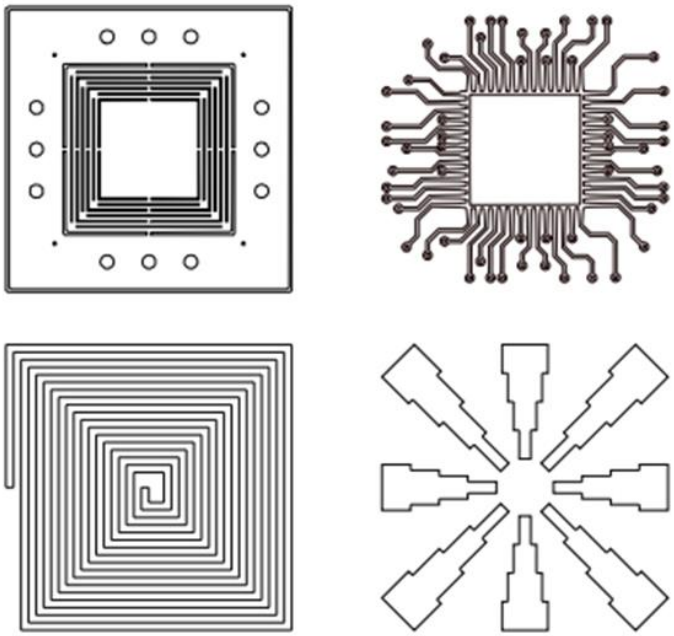

Fig (3-20) four pattern masks designed by AutoCAD.

3.3.3 Photosensitive

Photosensitive Dry Film 1 meter for Circuit Photoresist Sheet 30cm Width and cutting with needed size with Features of Universal usage in creating PCB board, attaching it on the glass surface to make it photosensitive, hole covering, and etching are all possibilities as shown in Fig (3-18). Excellent hole-covering ability, high resolution, and adaptability to various materials Durable under pH 8.0-8.5 conditions, 1.5 mils dry film fully covers a 0.25-inch height hole, are suitable for standard plating bath, also no wrinkle or color error. The steps for using Photosensitive Dry Film are as follows: Take off the cover, Clear the area, then attach the film carefully, be sure to make it flat and leave no air. To ensure precision, print the thin film or use parchment paper instead. To expose, place the printed design on the photosensitive board. The dry film will darken from pale blue to deep blue.

Fig (3.21) Photosensitive Dry Film 1 meter

3.3.4 UV Light.

UV Lamp can be used with 220V Sterilizer 8W T5 Tube as shown in Fig (3-19). the Specifications are: Wavelength: 253.7 nm, Germicidal UV Light Tube, T5

(G5) Lamp type, round tube Glass bulb type, with Disinfection area of 8W<=12m² and Tube length equal 31 cm.

Fig (3-22) UV Light Tube.

3.3.5 Universal PCB Developer.

Mix the can ingredients in 200 ml tap water in a suitable container. Moving it well with a plastic or glass rod until all the powder has dissolved. We can use warm water (approximately 50 c) to dissolve the powder faster, Allow the dissolvent to cool down and use between 20-25 c, depending on the strength of the solution and temperature. The developing time should range between 15-30 seconds, we wear gloves when working, we using a supplied container to measure the water required as shown in Fig (3-23).

Fig (3-23) Universal PCB developer.

3.3.6 Ferric Chloride (Fe2C13) For PCB Etching

Ferric chloride is most commonly used for etching PCB boards. Mix the solvent with warm water and your etching solution is ready. You can also store and reuse the solution. There are some Ferric Chloride Applications: such as Etching in Copper Clad Board and Art using Copper Clad Board.

3.3.7 Photolithography Implementation

In this work, it is needed to:

- form a positive film mask for microfabrication patterns because UV exposure decomposes a development inhibitor and developer solution dissolves negative photoresist in the exposed areas.
- Demolding after the etching is finished.
- Put the board into demolding water for several minutes.
- After the positive photoresist was put on a glass substrate, the substrate was then transferred to the 100°C oven and soft-baked for 10 minutes to drive out solvent from the layer for contact mask alignment. When the substrate

was cool down at room temperature, the resulting thickness changed. baking time is very important because photoresists are needed to sufficiently harden for developed photoresists after UV exposure. Soft baking techniques typically leave between 3 and 8% residual sensitivity in the resist film, which is enough to make the film stable throughout future lithographic processing.

- If the photoresist is not sufficiently hardened, the developer solution will remove all masked and unmasked photoresist layers. After making the soft-baking process, it is needed to expose UV with a patterned mask on a photoresist-coated substrate. A photoresist-coated substrate is put onto the wafer sample holder Single-side mask aligner. Then the patterned mask is put on the substrate. Then it is aligned to contact with the substrate and mask. After aligning the substrate and mask, it was exposed to UV for 3 minutes carried out in a Single-side mask aligner. In the alignment process, it is needed to align the mark on the mask and the mark on the wafer.
- An ultra-violet (UV) aligner is the most often utilized way of exposing features on a photoresist layer in microfabrication. The UV aligner requires a mask that comes into contact with a wafer and has characteristics that either block or transmit UV light. The UV aligner exposes a collimated UV light to ensure that features are accurately transmitted to a photoresist layer. The power output of the UV aligner varies with usage, Only the regions not shielded by the mask experience a chemical reaction between the resist and the light.
- The Wafer is baked again to ensure structure changes (20 – 30 minutes at (120 – 180 degrees), Mild Alkaline Solution Dissolves the Region of the

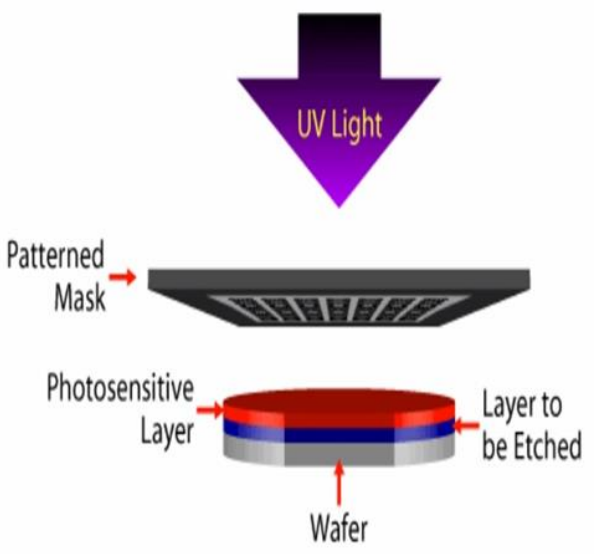

Fig (3-24) UV light shed on wafer [41]

photoresist, Photoresist coat elsewhere remains firm. The most commonly used photoresists are subaqueous-based elopers. After the exposure process was finished, the substrates were developed with developer solution for 10s and rinsed in DI water for 2 min. It is found that developing time depends on the exposure time and the strength of the developer.

- The resist-developer interactions have an impact on the geometry. Then we must clean the substrates, the substrates are soaked in acetone for 20 min and then soaked in DI water for 5 minutes. Then it is dried in an oven for 15 min at 100°C To be hardened. Pour the solution into a plastic container or dedicated etching tank, best results come out when the solution temperature is 45 C, Maximum etching temperature should not exceed 55 C, which depends on the strength of the solution and temperature.
- Place the substrate in etchants for 30 minutes. the photoresist layer is removed by immersing into the Photoresist remover (Acetone) for 3 minutes. Wash the substrate with isopropyl alcohol, then with distilled water, and then air dry.

Chapter Four
Results and Discussion

4.1 Introduction

This chapter presents and discusses the Practical results of This study and provides a simple and low-cost technique for rapid prototyping devices. It also describes enhancements to the original procedure, such as lower fabrication costs. The manufacture of a Low Cost Electronic Fabrication System has benefits such as the results can be attained similar to those obtained earlier by employing thermal evaporation devices with high vacuum pressures if we reduce the cost and make the technology available to everyone. This type of system is typically used to evaporate materials, although materials with higher melting points can be evaporated by reconfiguration of the boat that holds the evaporation material.

4.2 Thermal Evaporation Results and Discussion

The system achieves high vacuum via a rotary pump and is capable of achieving vacuum off in the ~ 10^{-6} bar range. Extremely low pressure is required to limit film oxidation and contaminant density. 10^{-6} bar is appropriate pressure, Lowering the pressures, on the other hand, would aid in reducing the density of pollutants in the film. At 10^{-6} bar the gas's mean free path gas in the chamber is around 0.53 m, typically referred to as the Knudsen number in the absence of a unit of measurement. In such cases, statistical methods should be used. The mean free path can be computed using the formula (2.1).

$$\iota = \frac{0.0000007}{0.0000013} = 0.53\, meter$$

Adhesion, friction, and wear can all have a significant impact on the efficiency, power production, and steady-state functioning of microelectronic devices. Adhesion and friction are also known to be affected by operational factors such as relative sliding velocity and environmental variables such as relative humidity and temperature. This has prompted the use of ultrathin lubricant coatings with low friction and adhesion for the protection of touching surfaces in microelectronic devices. Metallic films' interfacial adhesion to insulating substrates, such as glass, which is fundamentally low.

For the instance of the silicon substrate, the AFM patterns indicated a polycrystalline structure of monoclinic Cu & Al with a preferred orientation along the (111) planes. The AFM confirmed the direct creation of films. The joint action of intrinsic and thermal stresses was used to explain the fluctuation of crystallographic properties as a function of heating duration. The evaporation rate on the (silicon, glass, plastic) substrate evaluated here is relatively modest, the thin film thickness increased directly with the deposition rate.

4.3 AFM Results

AFM in tapping mode with Si tip cantilevers of $10^{-6}\ m$ symbolic bending was used to examine the copper & aluminium morphology and roughness of the surface.

4.3.1 Copper-Thin Films Deposited on a Glass Substrate

Fig (4-1) shows the glass substrate deposited by a pure copper. The deposited substrate with 2.5 cm length, 2.5 width and 0.2 thickness.

Fig (4-1) glass substrate deposited by copper

Fig (4-2) shows the AFM pattern of heated Copper thin layers deposited on glass substrate.

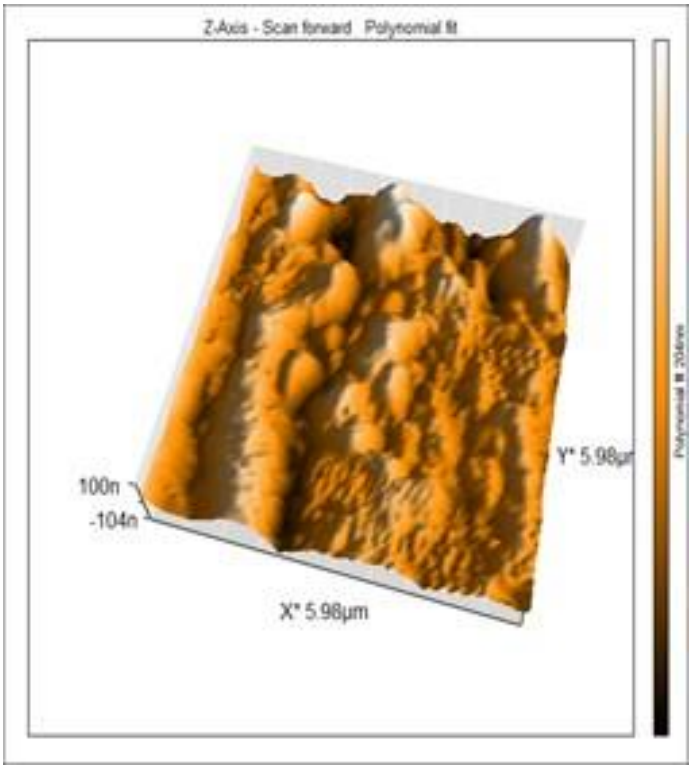

Fig (4-2) AFM pattern of the Cu thin films on glass.

The designs depict the many scattering peaks. Atomic force microscopy 2D and 3D AFM images of Cu thin film samples produced in this work with different thicknesses are given in Fig (4-3).

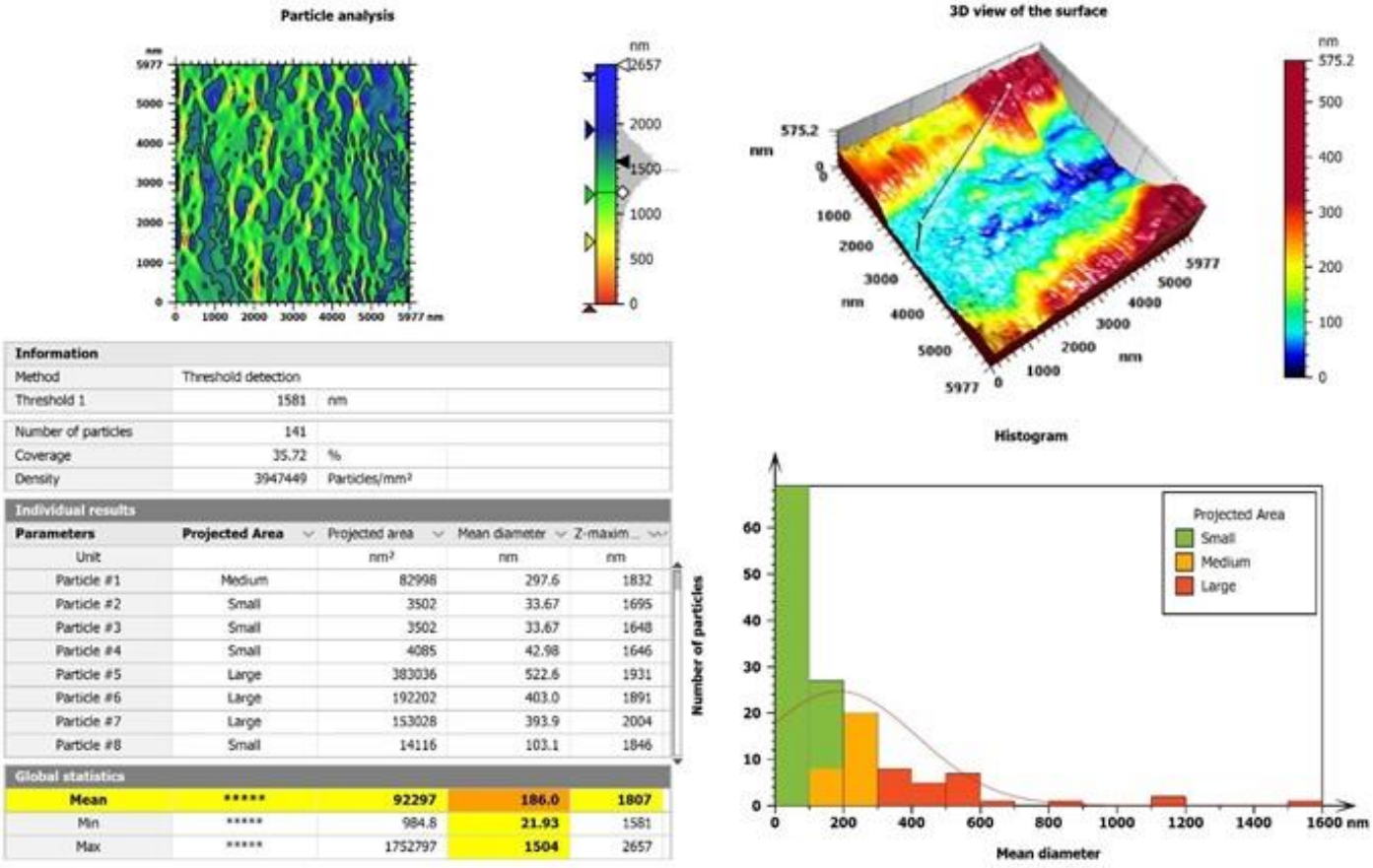

Information		
Method	Threshold detection	
Threshold 1	1581	nm
Number of particles	141	
Coverage	35.72	%
Density	3947449	Particles/mm²

Individual results				
Parameters	Projected Area	Projected area	Mean diameter	Z-maxim...
Unit		nm²	nm	nm
Particle #1	Medium	82998	297.6	1832
Particle #2	Small	3502	33.67	1695
Particle #3	Small	3502	33.67	1648
Particle #4	Small	4085	42.98	1646
Particle #5	Large	383036	522.6	1931
Particle #6	Large	192202	403.0	1891
Particle #7	Large	153028	393.9	2004
Particle #8	Small	14116	103.1	1846
Global statistics				
Mean	*****	92297	186.0	1807
Min	*****	984.8	21.93	1581
Max	*****	1752797	1504	2657

Fig (4-3) 3D view of the surface and mean diameter of copper on glass.

Fig (4-4) show the Histogram, Abbott curve and frequency and Z- maximum and mean height off, the number of particles is dependent on particle height was discovered that the copper deposits' adherence to glass weakened after a deposition time is below than 35 minutes owing to quick reactivity, which also emphasizes that current has a major influence on deposition rates.

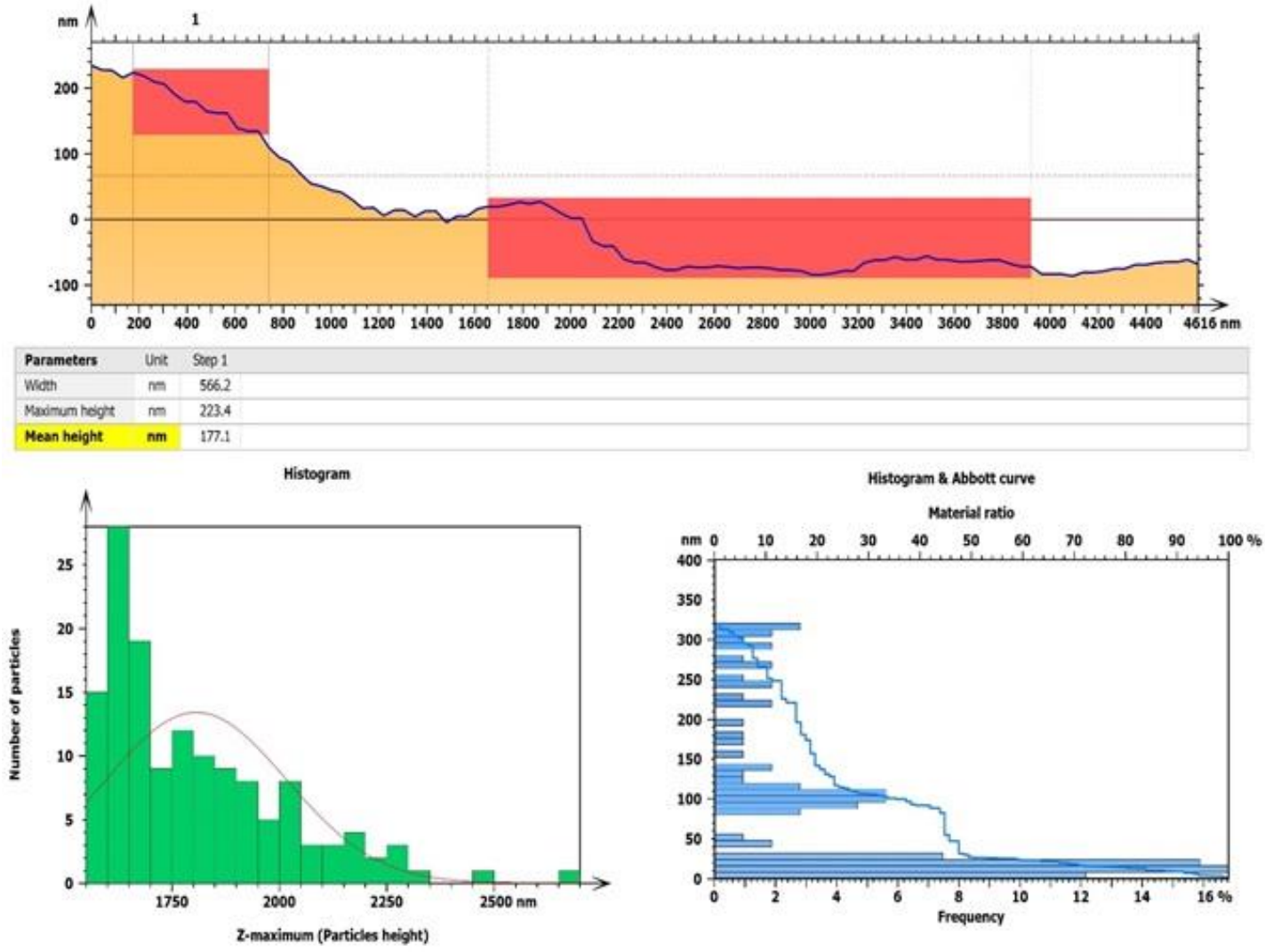

Fig (4-4) Histogram and frequency and Z- maximum of Cu thin films on glass.

AFM measurement on a surface of 0.5×0.5 μm2 indicated an average copper grain size, roughness is calculated on this surface. The surface was found to be smooth and free of visible copper particles after extremely short deposition periods (e.g., 20 minutes). When the deposition time was prolonged to 35 minutes, more particles developed on the surface, with a copper grain size on average of 114 nm and a size distribution is restricted. The grain size rapidly rose as deposition time passed. samples looked homogeneous and permanent throughout the surface after 35 minutes. roughness of the Cu that has been deposited which is determined and

estimated by pictures of AFM. Roughness rose as the Copper thickness grew from 114 nm to 375 nm as shown in Fig (4.5).

Height parameters				
Sq	**140.8**	**nm**		***Root-mean-square height***
Ssk	0.09144			*Skewness*
Sku	2.488			*Kurtosis*
Sp	437.4	nm		*Maximum peak height*
Sv	398.1	nm		*Maximum pit depth*
Sz	**835.5**	**nm**		***Maximum height***
Sa	**116.7**	**nm**		***Arithmetic mean height***
Functional parameters				
Smr	100.0	%	*c = 1000 nm below highest peak*	*Areal material ratio*
Smc	186.2	nm	*p = 10%*	*Inverse areal material ratio*
Sdc	356.3	nm	*p = 10%, q = 90%*	*Material ratio height difference*
Spatial parameters				
Sal	1479	nm	*s = 0.2*	*Autocorrelation length*
Str	*****		*s = 0.2*	*Texture-aspect ratio*
Std	180.0	°	*Reference angle = 0°*	*Texture direction*
Ssw	63.70	nm		*Dominant spatial wavelength*
Hybrid parameters				
Sdq	0.2954			*Root-mean-square gradient*
Sdr	4.151	%		*Developed interfacial area ratio*
Functional parameters (volume)				
Vm	5.474	nm³/nm²	*p = 10%*	*Material volume*
Vv	191.7	nm³/nm²	*p = 10%*	*Void volume*
Vmp	5.474	nm³/nm²	*p = 10%*	*Peak material volume*
Vmc	134.2	nm³/nm²	*p = 10%, q = 80%*	*Core material volume*
Vvc	179.0	nm³/nm²	*p = 10%, q = 80%*	*Core void volume*
Vvv	12.65	nm³/nm²	*p = 80%*	*Pit void volume*
Feature parameters				
Spd	1.511e-07	1/nm²	*Pruning = 5%*	*Density of peaks*
Spc	0.006338	1/nm	*Pruning = 5%*	*Arithmetic mean peak curvature*
S10z	688.8	nm	*Pruning = 5%*	*Ten point height*
S5p	336.9	nm	*Pruning = 5%*	*Five point peak height*

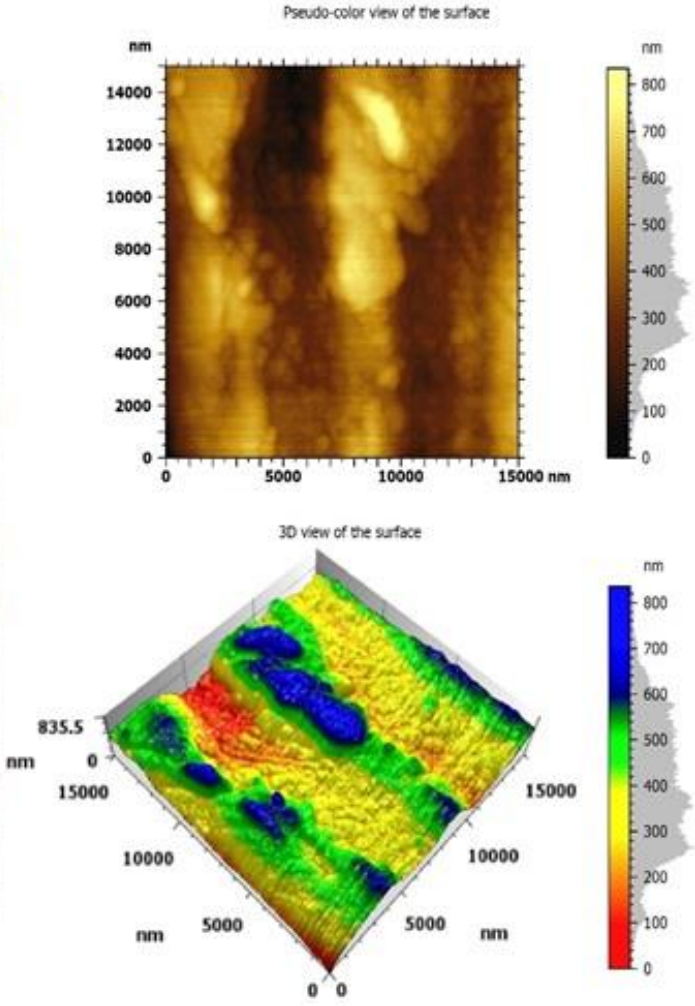

Fig (4-5) Roughness Analysis of copper deposited on a glass substrate

With increasing thickness, the grain size increased overall. The deposit surfaces' roughness is expected to grow with time of deposition in continuous films due to grain formation, which is consistent with many other results. The islands then grow in size until they collide and create a continuous film. Increasing deposition time, the film expansion will lead to fewer grain boundaries forming. the copper thicknesses grew with deposition time. The copper deposition thickness varies with

deposition time in the chamber and operating current. Starting the deposition below 120 amperes was quite challenging. the thickness of copper as a function of time deposition at 135 A. The realistic rate of deposition on the substrate of glass observed was quite modest. To illustrate how the substrate affects the deposition rate. The rate of deposition varied substantially amongst substrates, not merely due to varying currents. it seems that creating efficient nucleation sites on glass is more challenging than on the transparent the surface of substrate. As a result, 135 A is required for the next investigation to balance thickness and adhesive strength. The table (4.1) and Fig (4.6) show the thickness is increased directly by increasing time and no deposition bellow 135 A.

Table (4.1) thickness is increased directly by increasing time and no deposition bellow 135 A.

NO.	Time (min)	Thickness (nm)
1	0	0
2	5	0
3	10	0
4	15	0
5	20	0
6	25	0
7	30	45
8	35	114
9	40	375
10	45	515

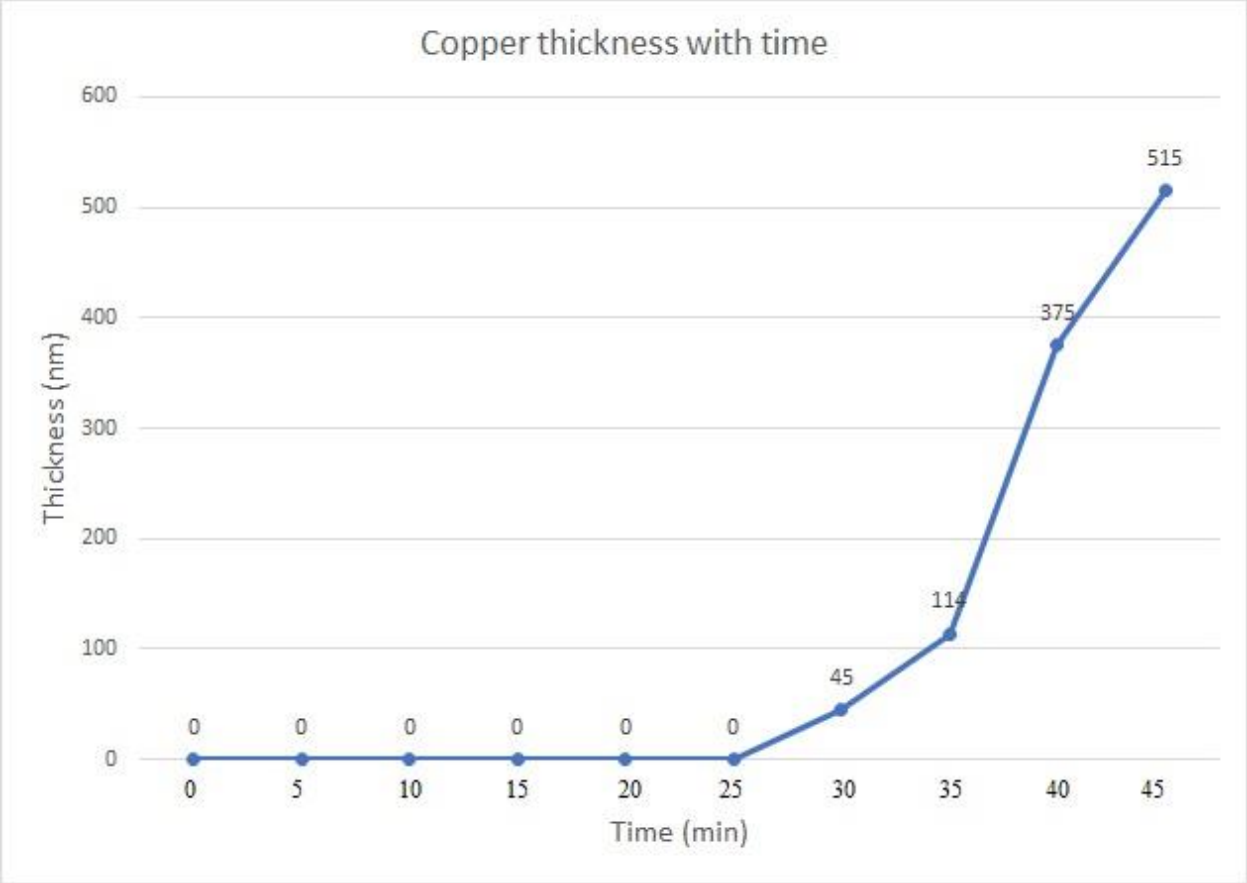

Fig (4-6) copper thickness with time.

4.3.2 Copper Deposited on a Plastic Substrate

Fig (4-7) shows the plastic substrate deposited by a pure copper. The deposited substrate with 2.5 cm length, 2.5 width and 0.2 thickness.

Fig (4-7) plastic substrate deposited by copper

Fig (4-8) shows the AFM patterns of heated Copper thin layers deposited on plastic substrate. The designs depict the many scattering peaks.

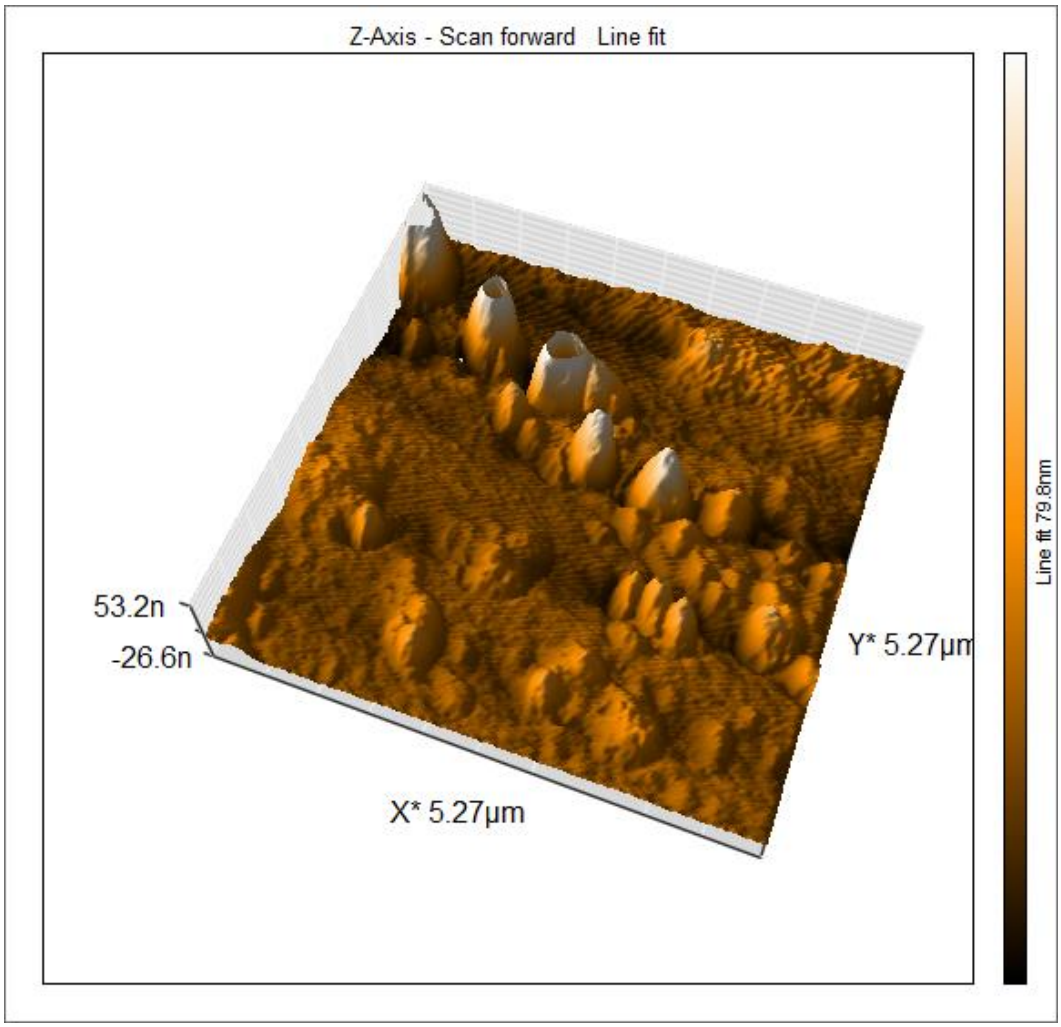

Fig (4-8) AFM pattern of the copper deposited on plastic substrate.

Atomic force microscopy 2D and 3D AFM images of Cu thin film samples produced in this work with different thicknesses are given in Fig (4-9)

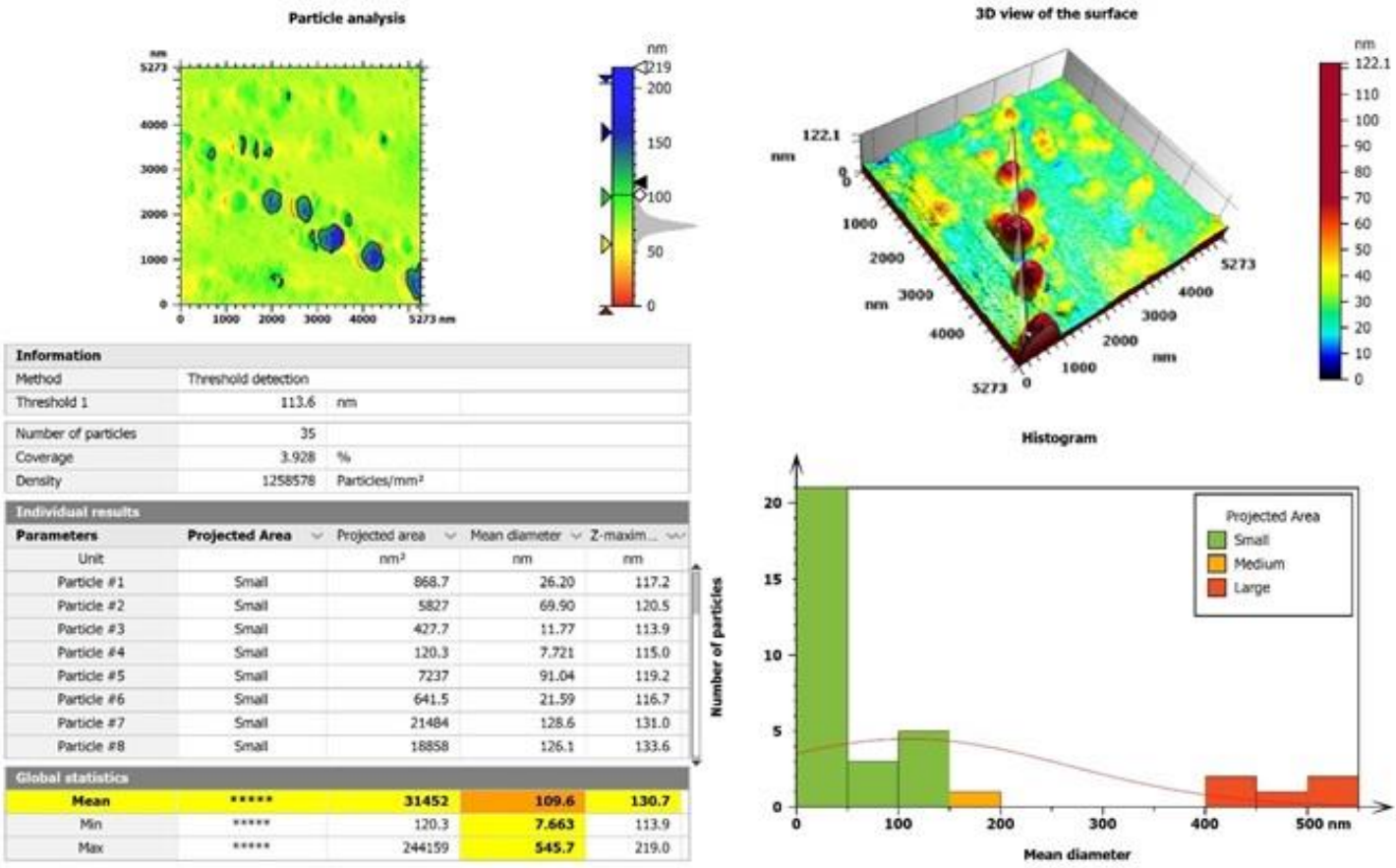

Fig (4-9) 3D view of the surface and mean diameter of copper deposited on Plastic substrate

Fig (4-10) that show the Histogram, Abbott curve and frequency and Z- maximum and mean height off, the number of particles is depend on particle height it was discovered that the copper deposits' adherence to plastic weakened after a deposition time is below than 35 minutes owing to quick reactivity, which also emphasizes that current has a major influence on deposition rates.

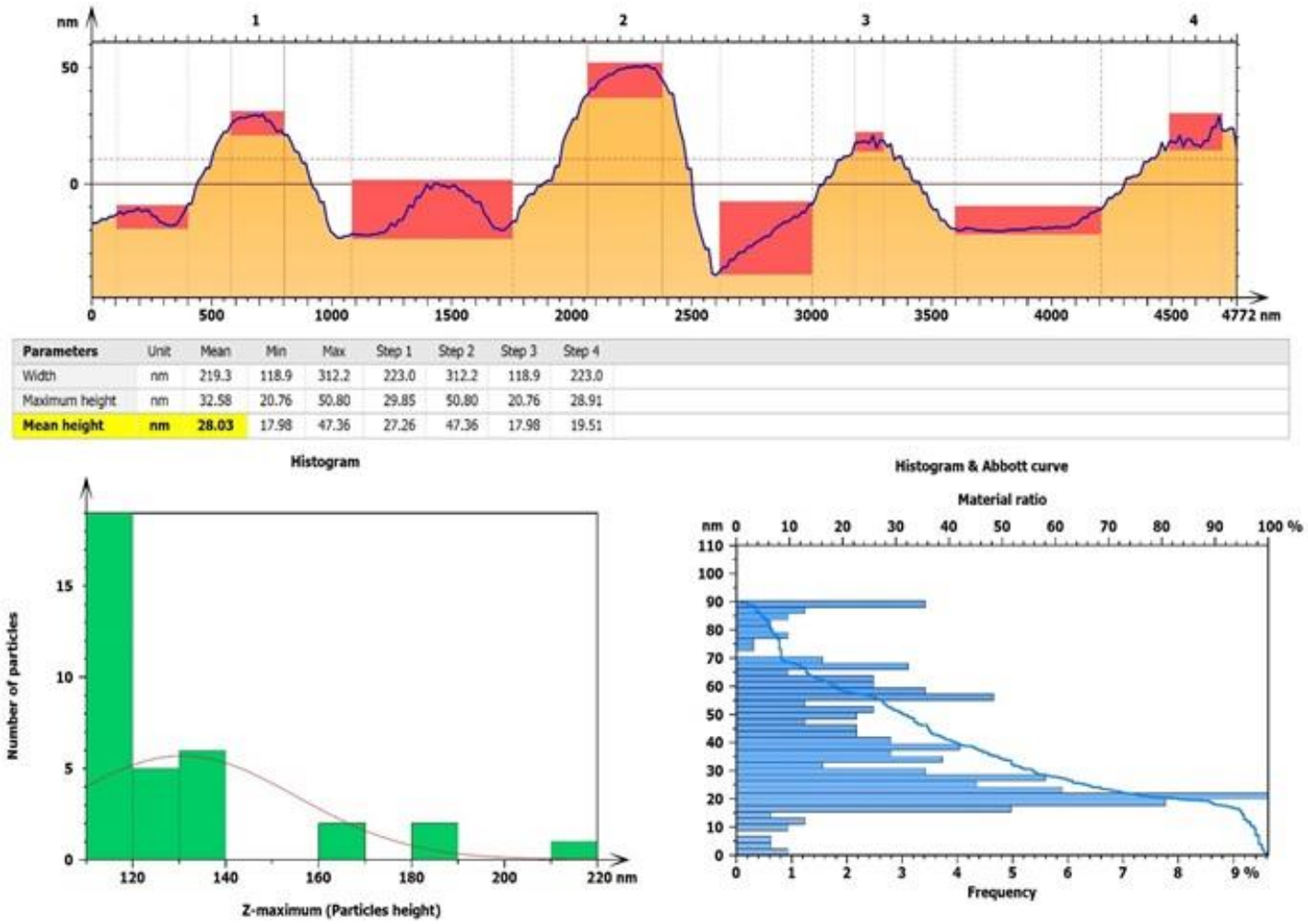

Parameters	Unit	Mean	Min	Max	Step 1	Step 2	Step 3	Step 4
Width	nm	219.3	118.9	312.2	223.0	312.2	118.9	223.0
Maximum height	nm	32.58	20.76	50.80	29.85	50.80	20.76	28.91
Mean height	**nm**	**28.03**	17.98	47.36	27.26	47.36	17.98	19.51

Fig (4-10) Histogram and frequency and Z- maximum of copper deposited on plastic substrate.

AFM measurement on a surface of 0.5×0.5 μm^2 indicated an average copper grain size. The surface was found to be smooth and free of visible copper particles after extremely short deposition periods (e.g. 20 minutes). When the deposition period was prolonged to 35 minutes, more particles developed on the surface, with a copper grain size on average of 123 nm and a size distribution restricted.

The film looked to be homogeneous and continuous throughout the surface at this point. After 45 minutes of evaporation, the copper particles had expanded in size and form, becoming polygonal. Using the system software, the roughness of the

copper that has been deposited is determined and estimated by pictures of AFM. roughness rose as the Cu thickness grew from 169 nm to 212 nm. Meanwhile, with increasing thickness, the grain size increased overall. The deposit surfaces' roughness is expected to grow with a time of deposition in continuous films due to grain formation.

Height parameters				
Sq	**12.40**	**nm**		***Root-mean-square height***
Ssk	2.289			*Skewness*
Sku	10.34			*Kurtosis*
Sp	75.66	nm		*Maximum peak height*
Sv	36.18	nm		*Maximum pit depth*
Sz	**111.8**	**nm**		***Maximum height***
Sa	**8.309**	**nm**		***Arithmetic mean height***
Functional parameters				
Smr	100.0	%	*c = 1000 nm below highest peak*	*Areal material ratio*
Smc	13.06	nm	*p = 10%*	*Inverse areal material ratio*
Sdc	23.94	nm	*p = 10%, q = 90%*	*Material ratio height difference*
Spatial parameters				
Sal	342.4	nm	*s = 0.2*	*Autocorrelation length*
Str	0.6373		*s = 0.2*	*Texture-aspect ratio*
Std	180.0	°	*Reference angle = 0°*	*Texture direction*
Ssw	29.86	nm		*Dominant spatial wavelength*
Hybrid parameters				
Sdq	0.1244			*Root-mean-square gradient*
Sdr	0.7450	%		*Developed interfacial area ratio*
Functional parameters (volume)				
Vm	1.568	nm³/nm²	*p = 10%*	*Material volume*
Vv	14.63	nm³/nm²	*p = 10%*	*Void volume*
Vmp	1.568	nm³/nm²	*p = 10%*	*Peak material volume*
Vmc	7.403	nm³/nm²	*p = 10%, q = 80%*	*Core material volume*
Vvc	13.96	nm³/nm²	*p = 10%, q = 80%*	*Core void volume*
Vvv	0.6628	nm³/nm²	*p = 80%*	*Pit void volume*
Feature parameters				
Spd	1.33e-06	1/nm²	*Pruning = 5%*	*Density of peaks*
Spc	0.006699	1/nm	*Pruning = 5%*	*Arithmetic mean peak curvature*
S10z	91.38	nm	*Pruning = 5%*	*Ten point height*
S5p	64.57	nm	*Pruning = 5%*	*Five point peak height*

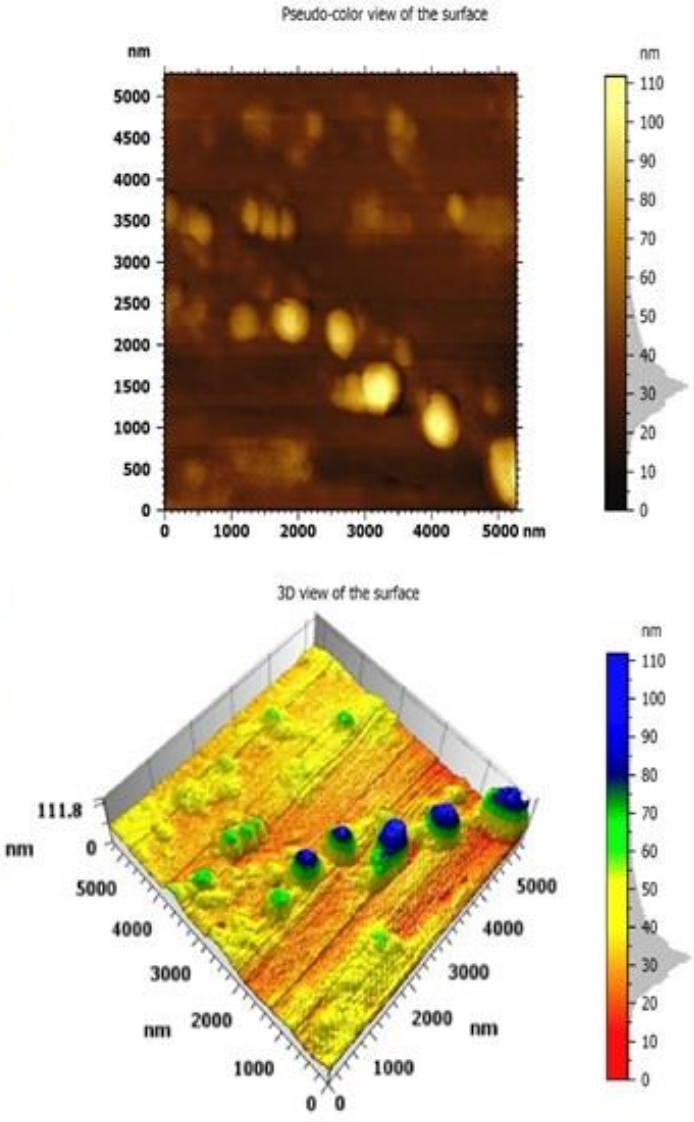

Fig (4-11) Roughness Analysis of Cu thin films deposited on plastic substrate

The islands then grow in size until they collide and create a continuous film. The copper deposition thickness varies with deposition duration in the chamber and

operating current. Starting the deposition below 125 amperes is quite challenging. The realistic rate of deposition on the substrate of plastic observed was quite modest, just around 212 nm thick in 45 minutes. To illustrate how the substrate affects the deposition rate. The rate of deposition varied substantially amongst substrates, not merely due to varying currents. As a result, 130 A is required for the next investigation to balance thickness and adhesive strength. The table (4.2) and Fig (4.12) show the thickness is increased directly by increasing time and no deposition bellow 130 A.

Table (4.2) thickness is increased directly by increasing time and no deposition bellow 130 A.

NO.	Time (min)	Thickness (nm)
1	0	0
2	5	0
3	10	0
4	15	0
5	20	0
6	25	0
7	30	41
8	35	123
9	40	169
10	45	212

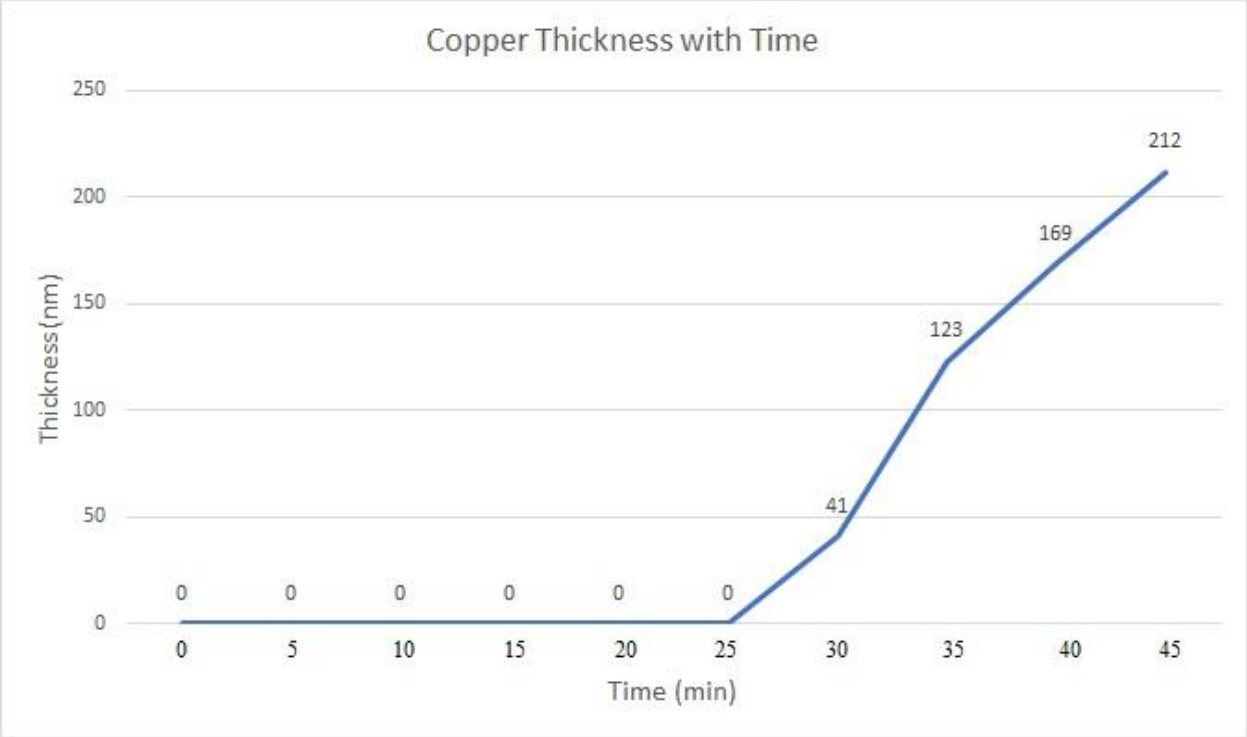

Fig (4-12) copper thickness with time.

4.3.3 Aluminum thin films deposited on a glass substrate

Fig (4-13) shows the glass substrate deposited by a pure Aluminum. The deposited substrate with 2.5 cm length, 2.5 width and 0.2 thickness.

Fig (4.13) Aluminum thin films deposited on a glass substrate

Fig (4-14) shows The AFM pattern of heated aluminum thin layers. The designs depict the many scattering peaks.

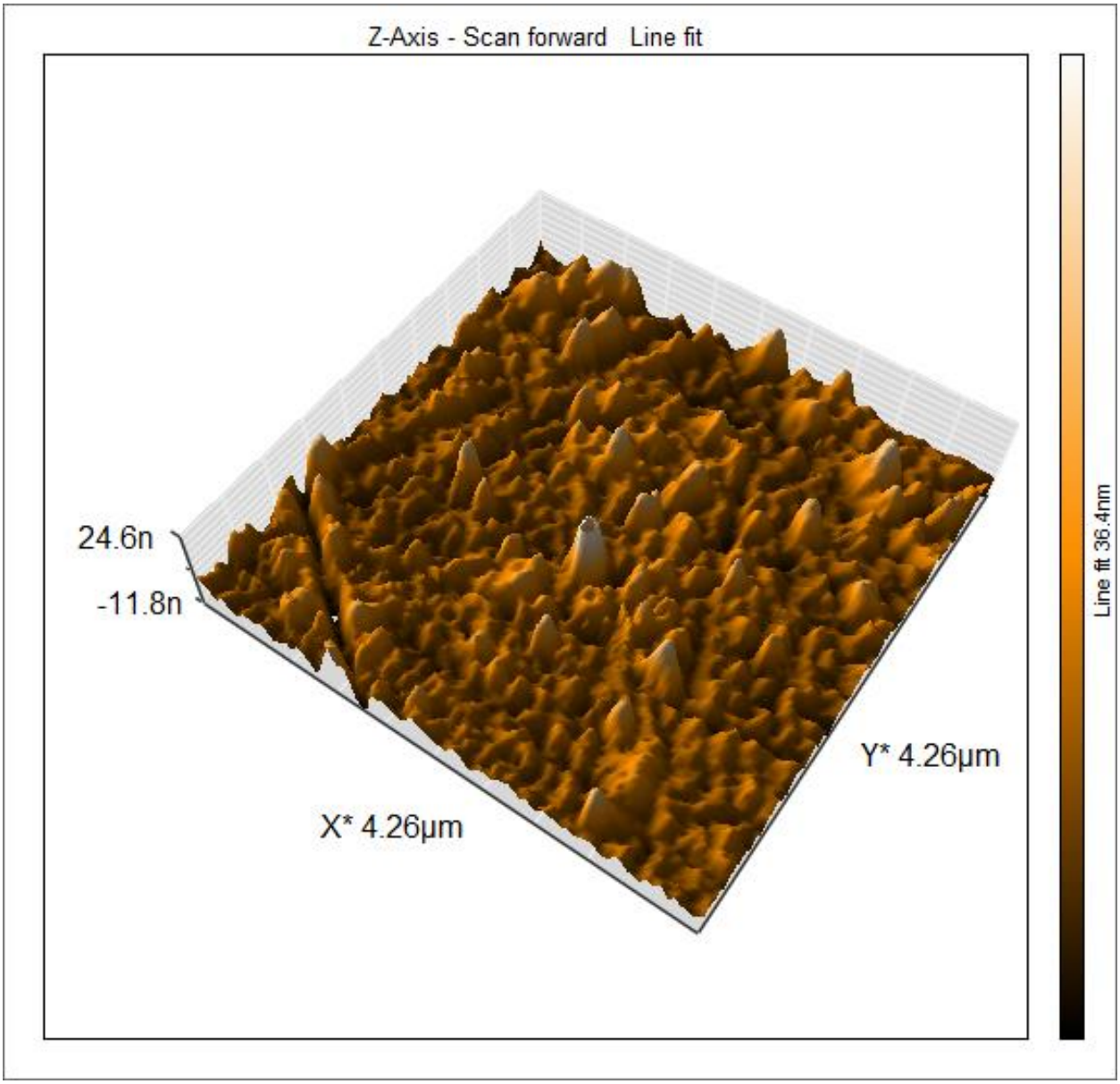

Fig (4-14) AFM pattern of the Aluminum thin films deposited on glass substrate.

Atomic force microscopy 2D and 3D AFM images of Al thin film samples produced in this work with different thicknesses are given in Fig (4-15).

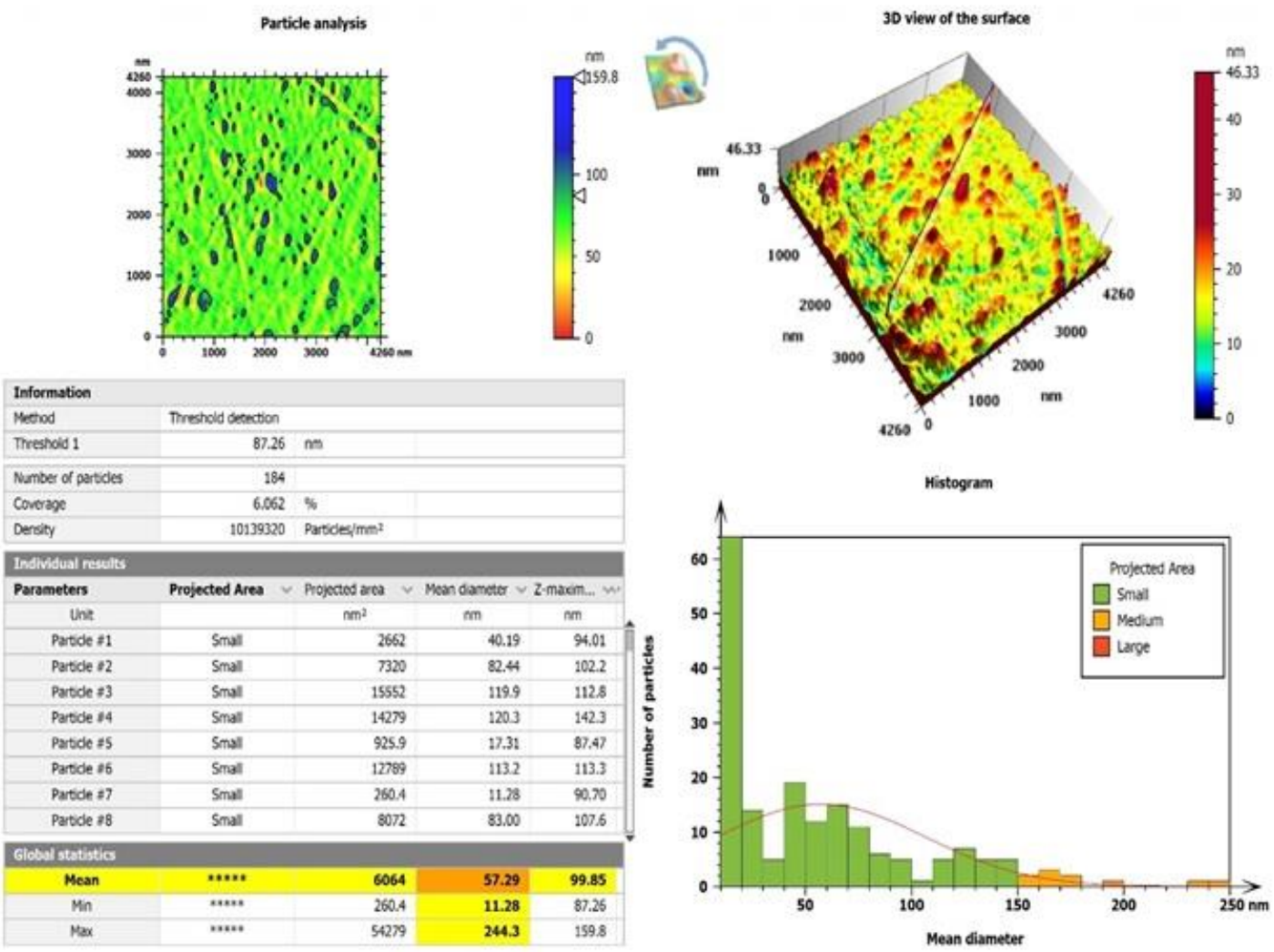

Information			
Method	Threshold detection		
Threshold 1	87.26	nm	
Number of particles	184		
Coverage	6.062	%	
Density	10139320	Particles/mm²	

Individual results				
Parameters	Projected Area	Projected area	Mean diameter	Z-maxim...
Unit		nm²	nm	nm
Particle #1	Small	2662	40.19	94.01
Particle #2	Small	7320	82.44	102.2
Particle #3	Small	15552	119.9	112.8
Particle #4	Small	14279	120.3	142.3
Particle #5	Small	925.9	17.31	87.47
Particle #6	Small	12789	113.2	113.3
Particle #7	Small	260.4	11.28	90.70
Particle #8	Small	8072	83.00	107.6
Global statistics				
Mean	*****	6064	57.29	99.85
Min	*****	260.4	11.28	87.26
Max	*****	54279	244.3	159.8

Fig (4-15) 3D view of the surface and mean diameter of aluminum on glass substrate.

Fig (4-16) shows the Histogram, Abbott curve and frequency and Z- maximum and mean height off, the number of particles is dependent on particle height was discovered that the interaction between aluminum deposits and glass had weakened once the deposition time was below than 35 minutes owing to quick reactivity, which also emphasizes that current has a major influence on deposition rates.

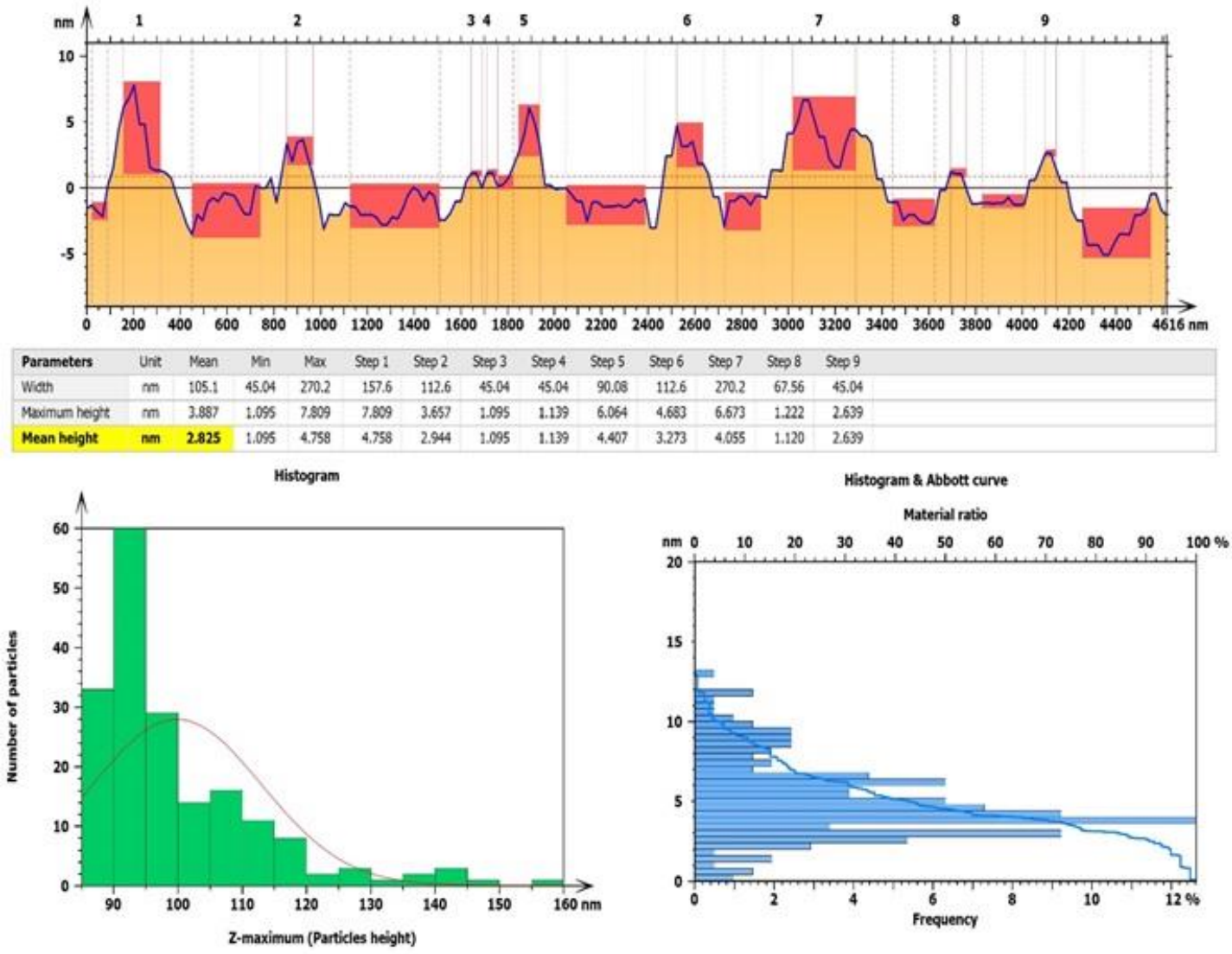

Parameters	Unit	Mean	Min	Max	Step 1	Step 2	Step 3	Step 4	Step 5	Step 6	Step 7	Step 8	Step 9
Width	nm	105.1	45.04	270.2	157.6	112.6	45.04	45.04	90.08	112.6	270.2	67.56	45.04
Maximum height	nm	3.887	1.095	7.809	7.809	3.657	1.095	1.139	6.064	4.683	6.673	1.222	2.639
Mean height	**nm**	**2.825**	1.095	4.758	4.758	2.944	1.095	1.139	4.407	3.273	4.055	1.120	2.639

Fig (4-16) Histogram and frequency and Z- maximum of aluminum on glass.

The average Aluminum pure wire AFM measurements on an area of 1000×1000 nm^2 were used to calculate sizes, roughness was evaluated. The surface was found to be smooth and free of visible Aluminum particles after extremely short deposition periods (e.g., 20 minutes). When the deposition period was prolonged to 30 minutes, more particles developed on the surface, with an aluminum wire size on average of 45 nm and a size distribution restricted. The wire size rapidly rose as deposition time passed, and within 45 minutes, aluminum granules were

determined to the range of 90-162 nm. The film looked to be homogeneous and continuous throughout the surface at this point. After 45 minutes of evaporation, the Aluminum particles had expanded in size and forms, becoming polygonal. Using the system software, the roughness of the Aluminum that has been deposited is determined and estimated by pictures of AFM. Roughness rose as the Aluminum thickness grew from 90 nm to 162 nm as shown in fig (4.17).

Height parameters				
Sq	**68.16**	**nm**		***Root-mean-square height***
Ssk	-0.5428			*Skewness*
Sku	3.221			*Kurtosis*
Sp	128.1	nm		*Maximum peak height*
Sv	216.1	nm		*Maximum pit depth*
Sz	**344.2**	**nm**		***Maximum height***
Sa	**54.04**	**nm**		***Arithmetic mean height***
Functional parameters				
Smr	100.0	%	*c = 1000 nm below highest peak*	*Areal material ratio*
Smc	93.81	nm	*p = 10%*	*Inverse areal material ratio*
Sdc	162.4	nm	*p = 10%, q = 90%*	*Material ratio height difference*
Spatial parameters				
Sal	644.1	nm	*s = 0.2*	*Autocorrelation length*
Str	*****		*s = 0.2*	*Texture-aspect ratio*
Std	180.0	°	*Reference angle = 0°*	*Texture direction*
Ssw	3865	nm		*Dominant spatial wavelength*
Hybrid parameters				
Sdq	0.3594			*Root-mean-square gradient*
Sdr	3.728	%		*Developed interfacial area ratio*
Functional parameters (volume)				
Vm	0.8590	nm³/nm²	*p = 10%*	*Material volume*
Vv	94.67	nm³/nm²	*p = 10%*	*Void volume*
Vmp	0.8590	nm³/nm²	*p = 10%*	*Peak material volume*
Vmc	61.67	nm³/nm²	*p = 10%, q = 80%*	*Core material volume*
Vvc	85.73	nm³/nm²	*p = 10%, q = 80%*	*Core void volume*
Vvv	8.935	nm³/nm²	*p = 80%*	*Pit void volume*
Feature parameters				
Spd	2.173e-07	1/nm²	*Pruning = 5%*	*Density of peaks*
Spc	0.01081	1/nm	*Pruning = 5%*	*Arithmetic mean peak curvature*
S10z	306.6	nm	*Pruning = 5%*	*Ten point height*
S5p	120.2	nm	*Pruning = 5%*	*Five point peak height*

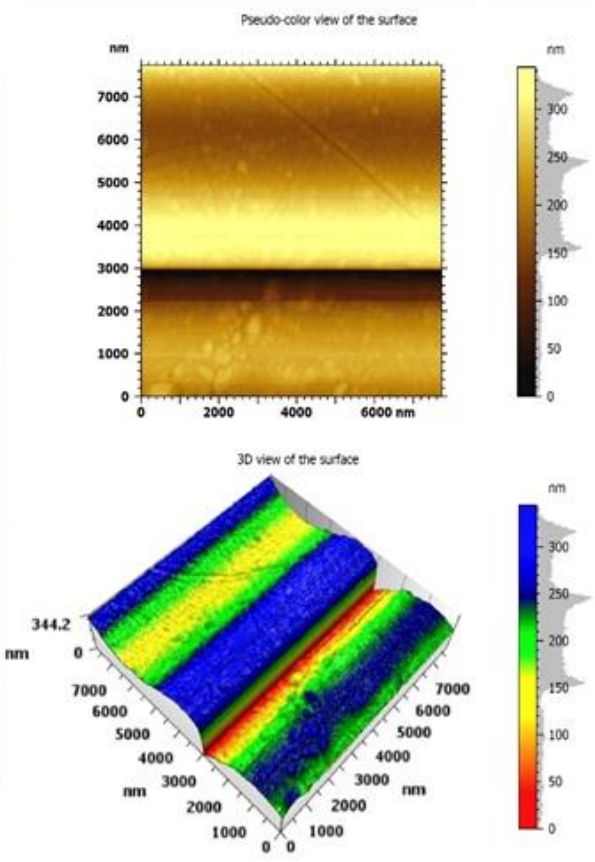

Fig (4-17) Roughness Analysis of Cu thin films deposited on plastic substrate

Meanwhile, with increasing thickness, the grain size increased overall. The deposit surfaces' roughness is expected to grow with time of deposition in continuous films due to grain formation, which is consistent with many other results. The islands then grow in size until they collide and create a continuous film. With increased deposition time, this film expansion leads to fewer grain boundaries forming.

The Aluminum deposition thickness varies with deposition duration in the chamber and operating current. Starting the deposition below 115 amperes was quite challenging. The realistic rate of deposition on the substrate of glass observed was quite modest, just around 212 nm thick in 45 minutes. It can be depicted from the result that the rate of deposition varied substantially amongst substrates, not merely due to varying currents. As a result, 120 A was chosen for the next investigation to regulate the thickness and strength of adhesion. Fig (4-18) shows images of the samples annealed under different pressures (a) samples annealed for 20 min (b) samples annealed for 35 min (c) samples annealed for 45 min. Table (4.3) shows thickness is increased directly by increasing time and no deposition bellow 120 A. Fig (4-19) shows copper thickness with time.

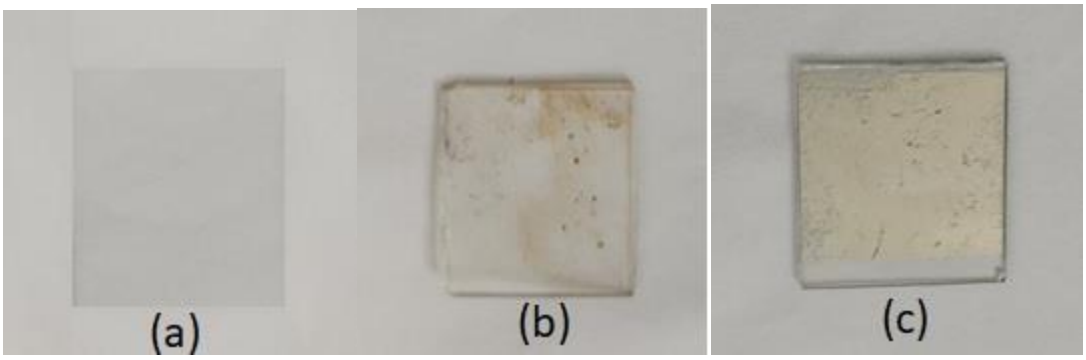

Fig (4-18) images of the samples annealed under different pressures (a) samples annealed for 20 min (b) samples annealed for 35 min (c) samples annealed for 45 min.

Table (4.3) thickness is increased directly by increasing time and no deposition bellow 120 A.

NO.	Time (min)	Thickness (nm)
1	0	0
2	5	0
3	10	0
4	15	0
5	20	45
6	25	90
7	30	162
8	35	212
9	40	295
10	45	336

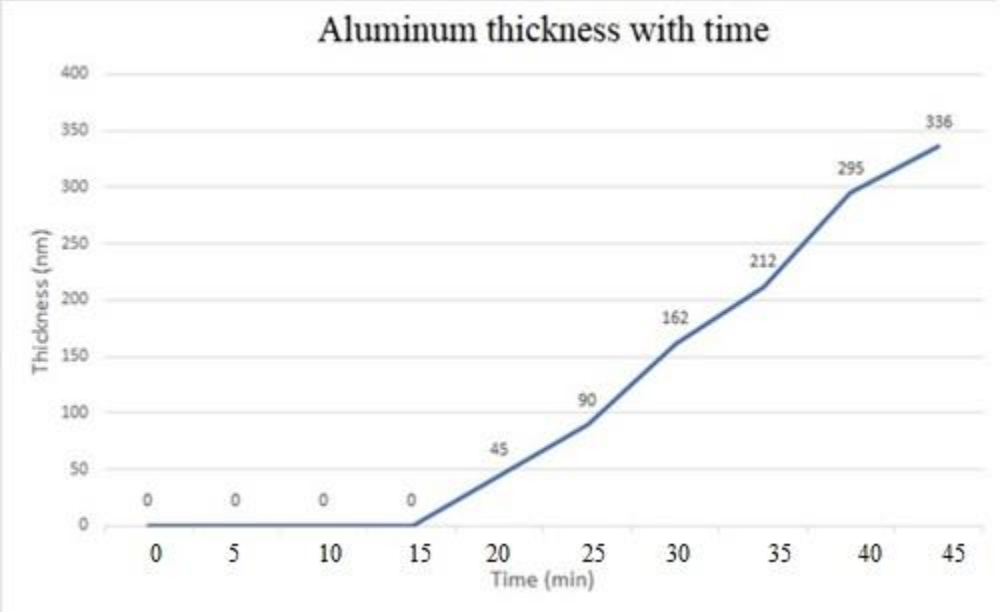

Fig (4-19) Aluminum thickness with time.

4.3.4 Aluminum thin films deposited on silicon substrate.

Fig (4-20) shows the silicon substrate deposited by a pure Aluminum. The deposited substrate with 2.5 cm length, 2.5 width and 0.1 thickness.

Fig (4-20) Aluminum thin films deposited on silicon substrate.

Fig (4-21) shows The AFM pattern of heated aluminum thin layers. The designs depict the many scattering peaks.

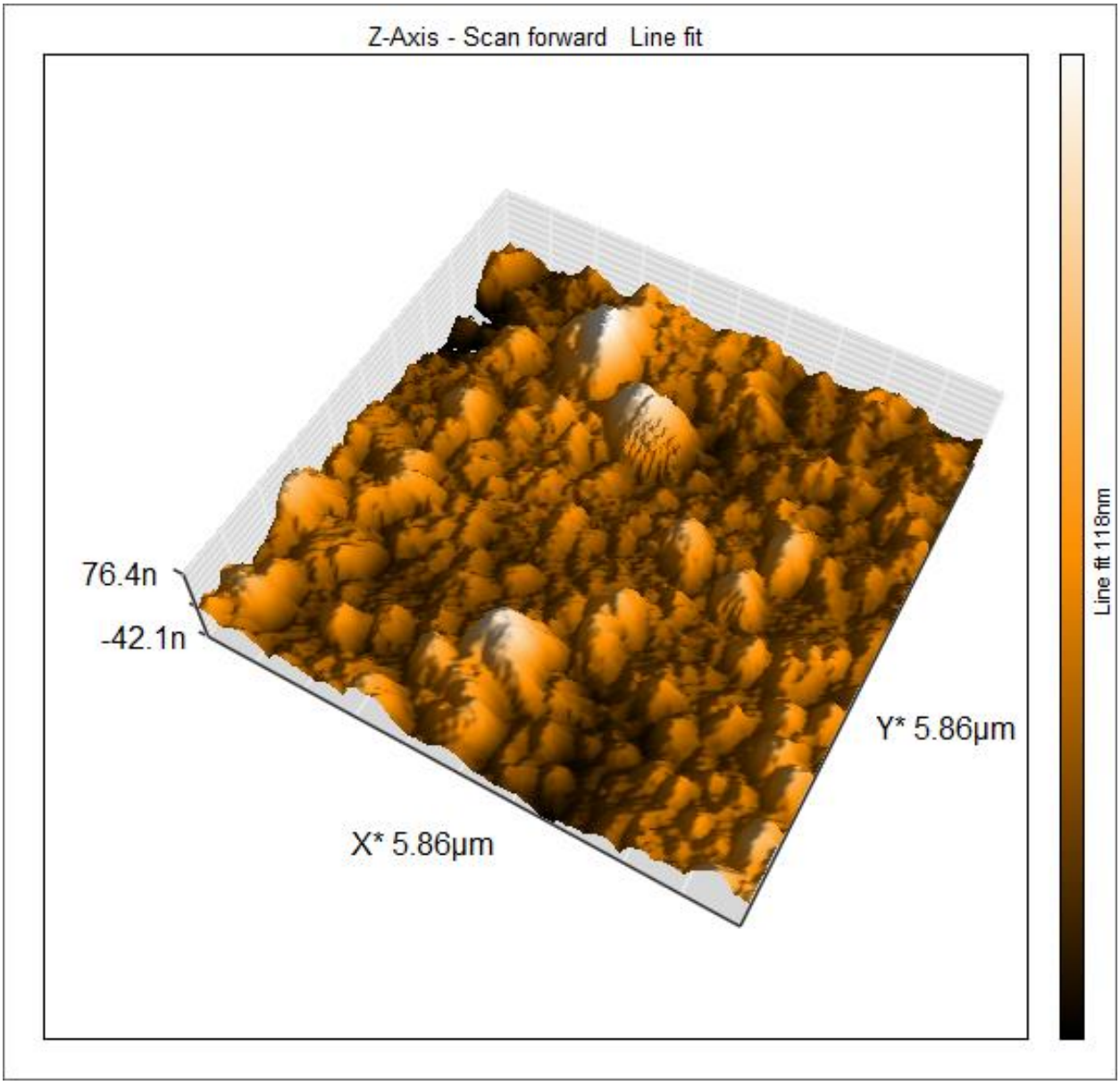

Fig (4-21) AFM pattern of the aluminum deposited on silicon.

Atomic force microscopy 2D and 3D AFM images of Al thin film samples produced in this work with different thicknesses and they give in Fig (4-22).

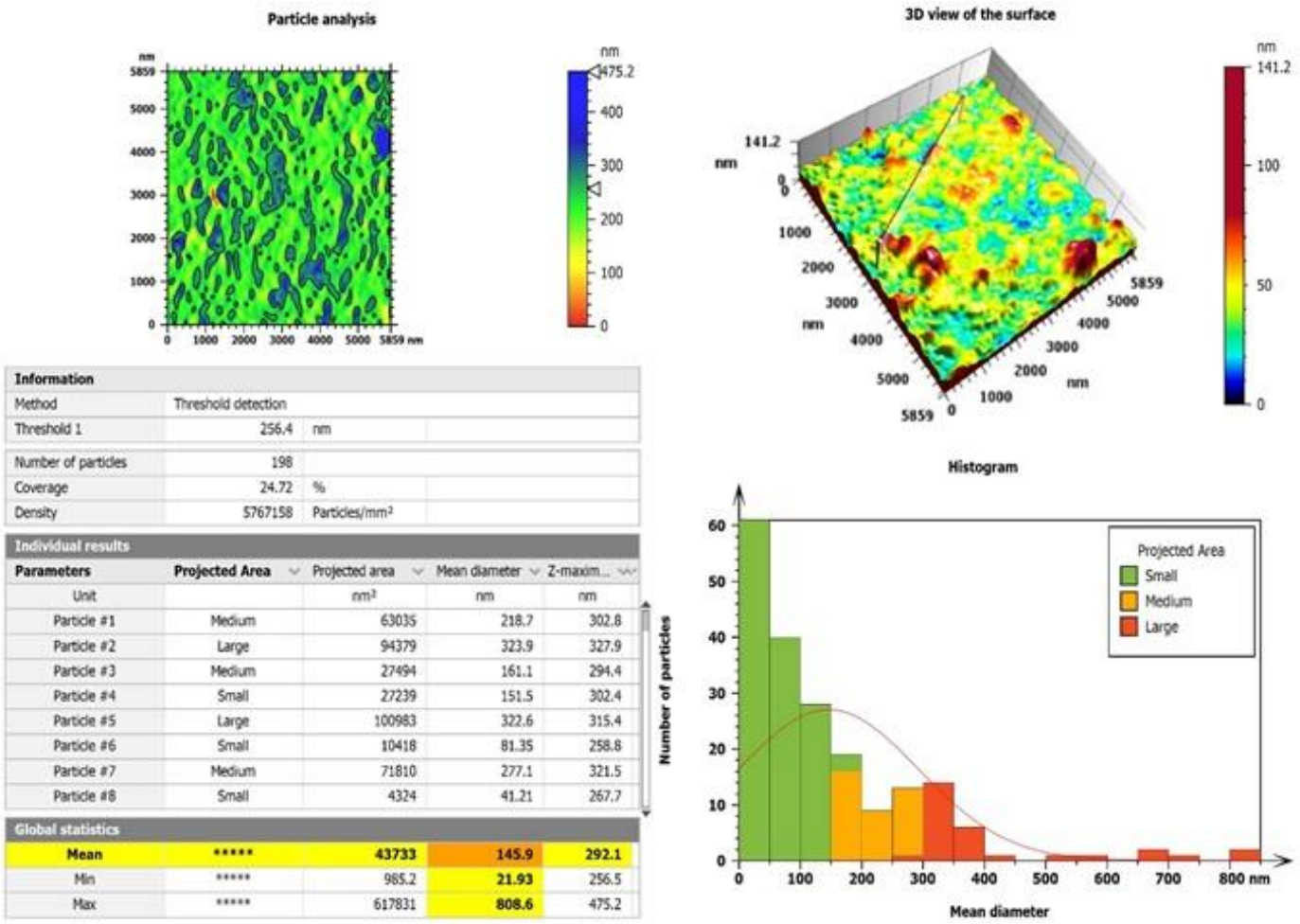

Information			
Method	Threshold detection		
Threshold 1	256.4	nm	
Number of particles	198		
Coverage	24.72	%	
Density	5767158	Particles/mm²	

Individual results				
Parameters	Projected Area	Projected area	Mean diameter	Z-maxim...
Unit		nm²	nm	nm
Particle #1	Medium	63035	218.7	302.8
Particle #2	Large	94379	323.9	327.9
Particle #3	Medium	27494	161.1	294.4
Particle #4	Small	27239	151.5	302.4
Particle #5	Large	100983	322.6	315.4
Particle #6	Small	10418	81.35	258.8
Particle #7	Medium	71810	277.1	321.5
Particle #8	Small	4324	41.21	267.7
Global statistics				
Mean	*****	43733	145.9	292.1
Min	*****	985.2	21.93	256.5
Max	*****	617831	808.6	475.2

Fig (4-22) 3D view of the surface and mean diameter of aluminum deposited on silicon.

Fig (4-23) shows the Histogram, Abbott curve and frequency and Z- maximum and mean height off, the number of particles is dependent on particle height was discovered that the interaction between aluminum deposits and silicon had weakened once the deposition time was below than 31 minutes owing to quick reactivity, which also emphasizes that current has a major influence on deposition rates.

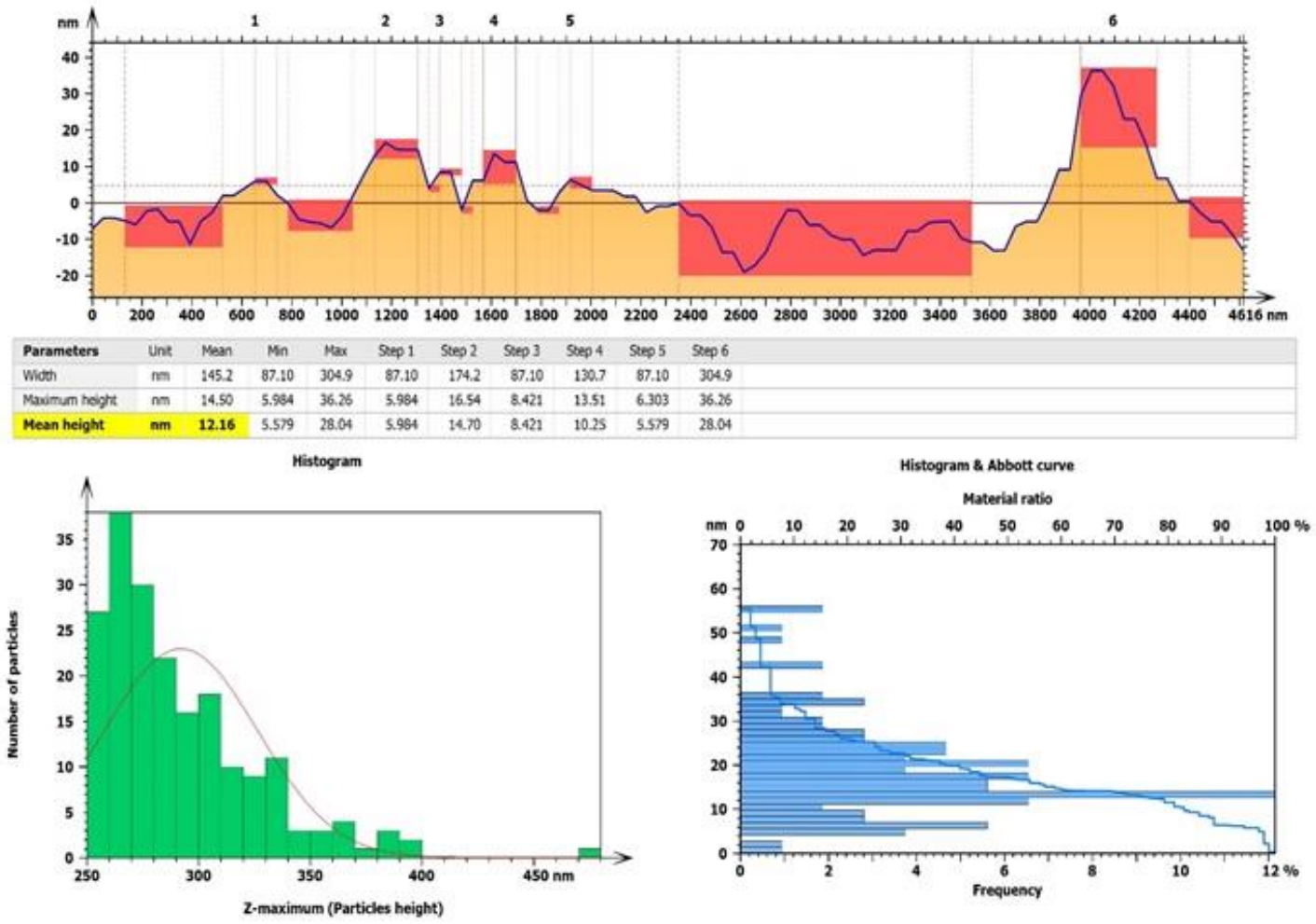

Fig (4-23) Histogram and frequency and Z- maximum of aluminum thin films deposited on silicon substrate.

The average Aluminum pure wire AFM measurements on an area of 1000×1000 nm^2. were used to calculate sizes, roughness was evaluated. The surface was found to be smooth and free of visible Aluminum particles after extremely short deposition periods (e.g. 16 minutes). When the deposition time was prolonged to 25 minutes, more particles developed on the surface, with an Aluminum wire size on average of 65 nm and a size distribution restricted. The wire size rapidly rose as deposition time passed, and within 45 minutes, Aluminum granules were determined to the range of 70-80 nm. The film looked to be homogeneous and

continuous throughout the surface at this point. After 45 minutes of evaporation, the Aluminum particles had expanded in size and form and becoming polygonal. Using the system software, the roughness of the Aluminum that has been deposited is determined and estimated by pictures of AFM. Roughness rose from 15 nm to 25 nm as the Aluminum thickness grew from 50 nm to 160 nm. Meanwhile, with increasing thickness, the grain size increased overall. The deposit surfaces' roughness is expected to grow with time of deposition in continuous films due to grain formation, which is consistent with many other results. The islands then grow in size until they collide and create a continuous film. With increased deposition time, this film expansion leads to fewer grain boundaries forming.

Height parameters				
Sq	**20.95**	**nm**		***Root-mean-square height***
Ssk	1.663			*Skewness*
Sku	9.979			*Kurtosis*
Sp	181.5	nm		*Maximum peak height*
Sv	65.68	nm		*Maximum pit depth*
Sz	**247.2**	**nm**		***Maximum height***
Sa	**15.15**	**nm**		***Arithmetic mean height***
Functional parameters				
Smr	100.0	%	*c = 1000 nm below highest peak*	*Areal material ratio*
Smc	23.70	nm	*p = 10%*	*Inverse areal material ratio*
Sdc	46.04	nm	*p = 10%, q = 90%*	*Material ratio height difference*
Spatial parameters				
Sal	1104	nm	*s = 0.2*	*Autocorrelation length*
Str	0.6081		*s = 0.2*	*Texture-aspect ratio*
Std	0.0001387	°	*Reference angle = 0°*	*Texture direction*
Ssw	84.94	nm		*Dominant spatial wavelength*
Hybrid parameters				
Sdq	0.1675			*Root-mean-square gradient*
Sdr	1.361	%		*Developed interfacial area ratio*
Functional parameters (volume)				
Vm	1.945	nm³/nm²	*p = 10%*	*Material volume*
Vv	25.65	nm³/nm²	*p = 10%*	*Void volume*
Vmp	1.945	nm³/nm²	*p = 10%*	*Peak material volume*
Vmc	15.46	nm³/nm²	*p = 10%, q = 80%*	*Core material volume*
Vvc	24.02	nm³/nm²	*p = 10%, q = 80%*	*Core void volume*
Vvv	1.625	nm³/nm²	*p = 80%*	*Pit void volume*
Feature parameters				
Spd	1.462e-06	1/nm²	*Pruning = 5%*	*Density of peaks*
Spc	0.003602	1/nm	*Pruning = 5%*	*Arithmetic mean peak curvat...*
S10z	194.4	nm	*Pruning = 5%*	*Ten point height*
S5p	139.6	nm	*Pruning = 5%*	*Five point peak height*

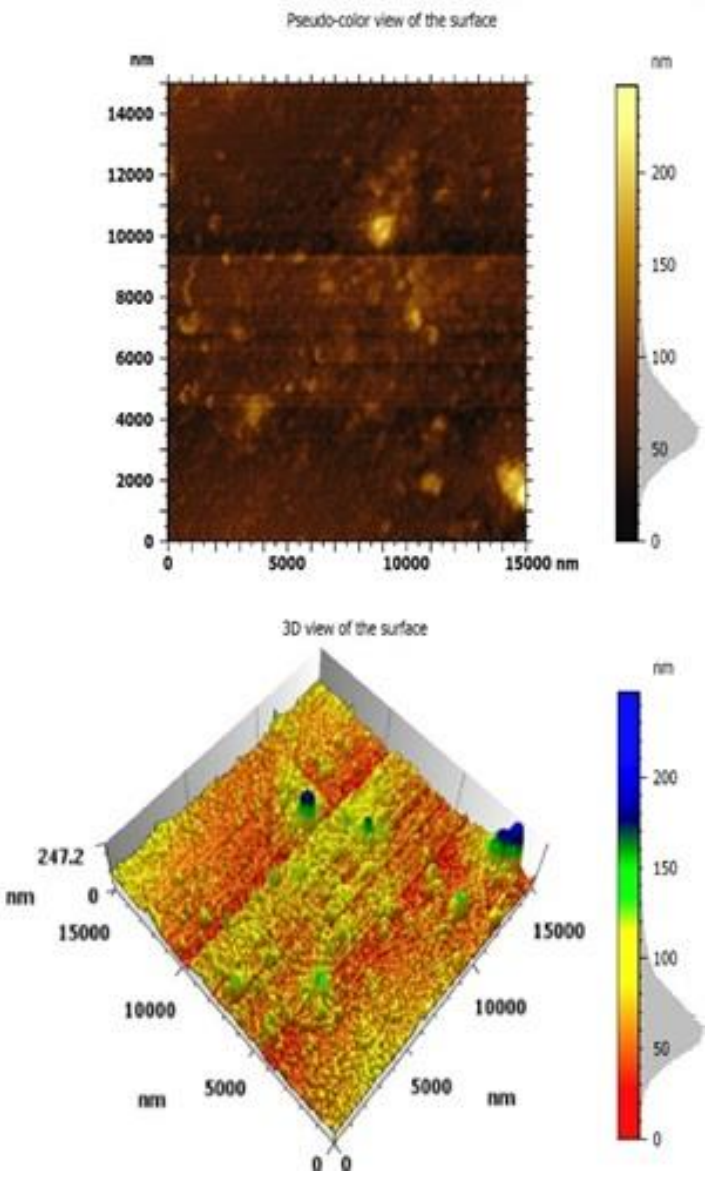

Fig (4-24) Roughness Analysis of aluminum deposited on silicon.

The Aluminum deposition thickness varies with deposition time in the chamber and operating current. Starting the deposition below 115 amperes was quite challenging. The realistic rate of deposition on the substrate of silicon observed was quite modest, just around 275 nm thick in 40 minutes. As a result, 120 A was chosen for the next investigation to regulate the thickness and strength of adhesion.

Table (4.4) shows thickness is increased directly by increasing time and no deposition below 120 A and Fig (4-25) shows Aluminum thickness with time.

Table (4.4) thickness is increased directly by increasing time and no deposition bellow 120 A.

NO.	Time (min)	Thickness (nm)
1	0	0
2	5	0
3	10	0
4	15	0
5	20	50
6	25	95
7	30	123
8	35	164
9	40	275
10	45	355

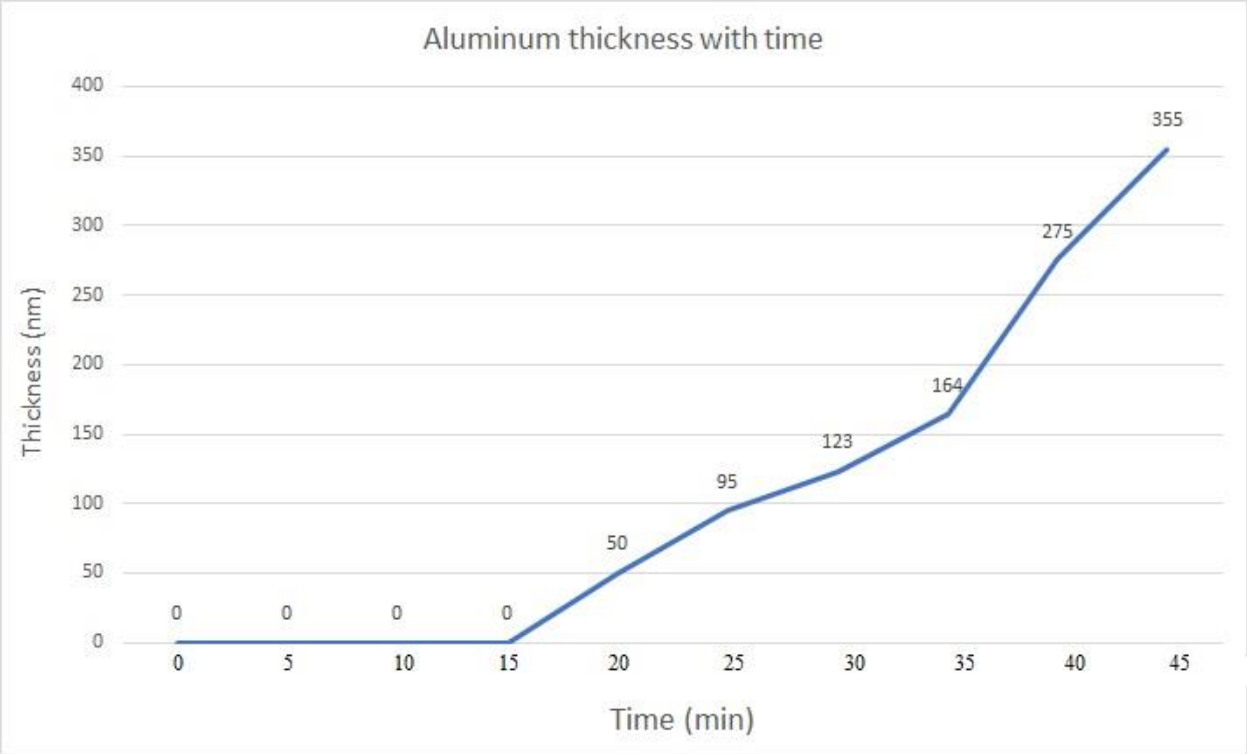

Fig (4-25) Aluminum thickness with time.

4.4 photolithography process results

Photolithography techniques are examined, and their importance in the manufacturing of microcircuits is outlined. The physical, chemical, and optical characteristics of photoresist materials are discussed in detail. Current optical pattern transfer production technologies are detailed, including contact printing, full wafer scanning projection, and direct wafer. The limitations of optical lithography are examined, as well as potential prospects. optimization of photolithography with the limited equipment that was available in this laboratory resulted in the ability to create microscale devices on-site. This can affect the capabilities of diverse research groups, as a wide variety of patterns and devices can now be designed and fabricated using similar methods and equipment. The resulting microfabrication patterns are given in Fig (4-26), the photo of microfabrication is illustrated. It is found that some patterns are clear and some are

not because of defects in mask patterns and decomposing during processing. There are found that some contamination in the images that are given in Fig (4-26) of the microfabrication pattern. It may be possible the contamination of the mask and residues of the photoresist and the laboratory is not dusting proof. And the goals of photoresist photo-sensitive coating are the correct thickness to reach good uniformity, and consistent lithographic response. Lithography limits are related to the wavelength of the radiation that exposes the photoresist. From the results we obtained, that the Excess solvent in photo-resist is driven out of the film by heat.

Photo-resist is further baked to remove the pin-holes and make it denser to facilitate the later etching step Photo-resist is removed by chemicals that can either dissolve or oxidize photo-resist.

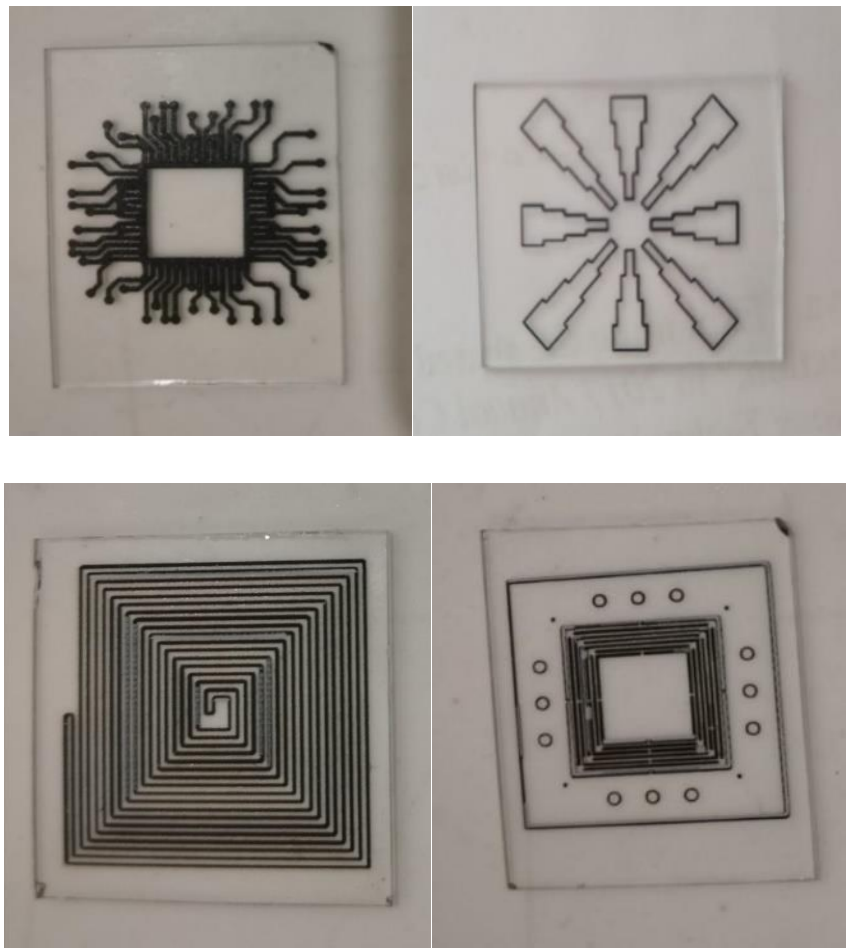

Fig (4-26) Resulting microfabrication patterns

4.5 Comparison of cost of microfabrication

Table (4-5) shows comparison between the proposed system, DV-502 Thermal Evaporator and Edward-C Thermal Evaporator.

parameters	The proposed system	DV-502 Thermal Evaporator [14]	Edward-C Thermal Evaporator [18]
Pressure (bar)	10^{-6}	10^{-8}	10^{-8}
Temperature	Need higher temperature	Need low temperature	Need lower temperature
Power supply	complex	moderate	Simple
Cooling system	Simple	Complex	Complex
Current	Need about 135 A	Need about 60 A	Need about 40 A
Cost	Low cost (4000 $)	high cost (25000 $)	high cost (30000 $)
Deposition time	More than 35 minutes	Less than 20 minutes	Less than 15 minutes

Through the results obtained and through comparisons made with other devices, the device used gives similar results with a higher current, lower pressure, a less complex cooling system, and a larger power supply unit. The cost comparison of standard microfabrication and our low-cost microfabrication method is depicted in this section. It estimates the cost for a one-time microfabrication process. It is found that the low-cost fabrication method is very low in mask-making processes. And it is also found that microfabrication patterns have been successfully fabricated. The table (4-6) shows a comparison between the proposed Low-cost photolithography and the Standard photolithography.

Table (4-6) comparison between the proposed Low-cost photolithography and the Standard photolithography.

Parameter	The proposed photolithography	Canon FPD Lithography [46]
Size of device	Small size	Big size
UV light	Simple	Big and complex
Mask	Emulsion mask (low cost)	Chrome mask (high cost)

Through the results obtained and through comparisons made with Standard photolithography, the device used gives similar results with a smaller size, simpler UV light, lower cost emulsion mask, and Photosensitive Dry Film with a lower cost of 5 dollars.

Chapter Five

Conclusions and Future Works

5.1 Conclusions

- Physical vapor deposition is a Line of line-of-sight process, Which Means it is not Ideal for Coating Nonvisible Surfaces.
- We found that the proposed low-cost fabrication is cost-effective for rapid prototyping.
- Economic considerations are critical.
- Atomic forces microscopic (AFM) shows the roughness increased with increasing thickness.
- The microstructure of copper coatings on glass was studied as a function of deposit thickness. The results showed that the first development of the metallic copper layer onto catalytic nucleation sites is a critical phase in the deposition process in terms of microstructure.
- Various elements, such as contamination, adhesion, exposure rate, sensitivity, and exposure source, affect photoresist performance.
- Minimizing the substrate area, the resolution is lower and the more difficult is exceeded.
- Negative Photoresist is Cheaper with poor resolution while Positive Photoresist is Expensive with better resolution.
- Temperature can influence photoresist viscosity.
- No deposition getting when current below 115 A.
- No deposition getting when deposition time is below 30 minutes.

- Aluminum deposition needs current less than copper deposition because of the evaporation temperature of aluminum is lower than the evaporation temperature of copper.
- Through the results obtained and through comparisons made with other devices, the device used gives similar results with a higher current, lower pressure, a less complex cooling system, and a larger power supply unit.

5.2 Future Works

- Preparing the thin films by thermal evaporation technique with lower temperatures.
- Preparing the thin films by thermal evaporation technique with lower time.
- Manufacturing a thermal evaporator with a higher electrical power supply.
- Manufacturing a thermal evaporator with a higher with a higher-pressure vacuum pump.

References

[1] D. Dastana, K. shanb, "Influence of heat treatment on H2S gas sensing features of NiO thin films deposited via thermal evaporation technique", Elsevier: vol. 4, pp. 98-102, February 2023.

[2] S. Mohammad, F. Mesgari, "Electro chemiluminescence Sensors based on Lanthanide Nanomaterials as Modifiers", Elsevier, Volume 18, Issue 1, pp.45-51, 2022.

[3] Zainab Qassim Mohamed; Abdul Azeez O. Mousa Al-Ogaili; Khalid Hanen Abbas; "Morphology and optical properties of Cu_2O-Doped CuO nano films prepared via thermal evaporation technique", AIP Conf. Proc Volume 2475, Issue 1,pp. 154-159, (2023).

[4] J. Olofsson, J. Gerth, H. Nyberg, U. Wiklund, S. Jacobson, "On the influence from micro topography of PVD coatings on friction behaviour, material transfer and tribe film formation", Elsevier, Volume 271, Issues 9, pp. 2046-2057, 29 July 2011.

[5] H. M. Ali, I. H. Khudayer, "Influence Annealing on the Physical Properties of Silver Selenide Thin Film at Different Temperatures by Thermal Evaporation", IHJPAS. Vol. 36, Issue 2, 2023.

[6] D. Mattox, "The foundations of vacuum coating technology". Noyes Publications, pp.151-180, 2018.

[7] H. Jawad Kadim, H. Al-Mumen, H. Nahi, "Tunable plasmon-induced transparency in one-dimensional gold nano-grating as a new kind of neuro-transmitter sensor". Elsevier, vol. 269, 2022.

[8] K. Dhivakar, A. Sarje, "A Versatile, Low-Cost UV Exposure System for Photolithography, " Smart Technologies, Communication and Robotics, pp 29-33,2021.

[9] D. Abdel- Monem, S. A. Aly, M. Abdel-Rahman, and E. R. Shaaban, " Effect of heat treatment in structural and optical properties of 1 μ of Cu/CdTe thick film". International Journal of New Horizons in Physics.10, No. 1, 11-20, Jan. 2023.

[10] V. Travkin, Yu. Sachkov, Koptyaev, G.L. Pakhomov, "Isomer-dependent performance of thin-film solar cells based on petro porphyrins". Elsevier Chemical Physics, Volume 573, 1 September 2023.

[11] E.M. El-Zaidia, R. Bousbih, A. Darwish."Effect of film thickness on structural, electrical and optical properties of amorphous boron subphthalocyanine chloride thin film", Elsevier. Optical Materials, Volume 138, April 2023

[12] Rajendra Kumar Goyal, "Nanomaterials and Nanocomposites Synthesis, Properties, Characterization Techniques, and Applications", Taylor & Francis Group, Boca Raton London New York, (2018).

[13] Panjan, P.; Drnovšek, A; Kovač, J. "Tribological aspects related to the morphology of PVD hard coatings". Surf. Coat. Technol. 2018.

[14] Xiaoyun Cui, David A. Hutt, "Evolution of microstructure and electrical conductivity of electroless copper deposits on a glass substrate", Thin Solid Films, July 2012.

[15] I. Hossain, "prospects of CZTS solar cells from the perspective of material properties, fabrication methods and current research challenges". chalcogenide Lett, vol. 9, no. 6, 2012.

[16] Biswal, Sameer Ranjan. "Structural and Optical Study of Pure CuI Thin Film by Horizontal Thermal Evaporation" Technique 8th Edition of International Conference on Nanotechnology for Better Living (ICNBL), NIT Srinagar, 25-29 May 2023.

[17] R. Voyce, S. Campbell, S. Hutter, G. Zoppi, N. Beattie, E. Gibson, V. Barrioz; "Exploring the Role of Temperature and Hole Transport Layer on the Ribbon Orientation and Efficiency of Sb2Se3 cells Deposited via Thermal Evaporation"

Photovoltaic Specialists Conference 2022.

[18] H. Rekkache, H. Kassentini, L. Bechiri; "Study of Copper Tin Selenide Nanoparticles of Milled Powder and Thin Films", Journal of Nano Research 21 March 2022.

[19] R. Doering N. Yoshio "Handbook of Semiconductor Manufacturing Technology". CRC Press: Boca Raton,21-25; 2007.

[20] C. YH, Shi X, Tan HS. "Influence of substrate bias on the microstructure and internal stress in Cu films deposited by filtered cathodic vacuum arc". Journal of Vacuum Science & Technology A: Vacuum, Surfaces, and Films, 2016.

[21] H Al-Mumen, "Optoelectronic Properties of Dome-Shaped Substrate UV Detector with Optical Coating", International Journal of Applied Engineering Research 11 (16), 8916-8919 5 2016.

[22] Yu M, Zhang J, Li D, Meng Q, Li W. "Internal stress and adhesion of Cu film/Si prepared by both MEVVA and IBAD". Surface and Coatings Technology. 2006.

[23] Nashreen F. Patel, Sanjay A. Bhakhar, Hiren S. Jagani "Synthesis, characterization and optoelectronic application of Bi_2Se_3 thin film prepared by thermal evaporation technique" V.136, 2023.

[24] Hiba M. Ali, I. Khdair. "Preparation and analysis of Ag2Se1-xTe x thin film structure on the physical properties at various temperatures by thermal evaporation". chalcogenide-letters, p. 197 – 203, 2023.

[25] I. Guler, M. Isik N. Gasanly Structural and optical properties of $(TlInS_2)_{0.75}$ $(TlInSe_2)_{0.25}$ thin films deposited by thermal evaporation" Journal of Materials Science: Materials in Electronics, volume 34, 2023

[26] D. Dastan, Ke shan, Azadeh Jafari, Tomasz Marszalek: "Influence of heat treatment on H2S gas sensing features of NiO thin films deposited via thermal evaporation technique". Elsevier, vol 154, 2023.

[27] H Al-Mumen, W Li, "Complementary metal-SU8-graphene method for making integrated graphene nanocircuits Micro & Nano Letters", 13 (4), 465-468 6 2018.

[28] M. Al-Essa and Ahmed Jumma Noori, "DC conductivity of PbxSe1-thin films prepared by thermal evaporation technique", Pelagic Research Library, Advances in Applied Science Research, (2014).

[29] H. Frey, H.R. Khan, "Applications and Developments of Thin Film Technology", Handbook of Thin-Film Technology, Springer-Verlag Berlin Heidelberg, (2015).

[30] A.Julio, T. Soares, M. Sardela;" Practical Materials Characterization", Springer Science Business, University of Illinois at Urbana-Champaign Media New York, 43, (2014).

[31] Hidekazu Tanaka, "Handbook of Crystal Growth"; Thin Films and Epitaxy (Second Edition),pp .26-31. 2015.

[32] O. Stenzel, "The physics of thin film optical spectra". Springer, pp.143-156.2016

[33] Z. Wang, Zongrong, Xiaochen "Low Cost Universal High-k Dielectric for Solution Processing and Thermal Evaporation Organic Transistors" Materials Science Advanced Materials Interfaces, semantic scholar 2014.

[33] A. Jilani, M. Shaaban Abdel-Wahab, "Advance Deposition Techniques for Thin Film and Coating, Modern Technologies for Creating the Thin-film Systems and Coatings", pp.11-14, (2017).

[34] M. Benelmekkia, A. Erbeb, "Nanostructured thin films-background, preparation and relation to the technological revolution of the 21st century", NTNU, Norwegian University of Science and Technology", Trondheim, Norway, Frontiers of Nanoscience Volume 14, pp. 1-34, 2019.

[35] D. Jameel, "Thin Film Deposition Processes", International Journal of Modern Physics and Applications Vol. 1, No. 4, pp. 193-199, (2015).

[36] W. Kyung, E. Whitener, "Transferring photolithography patterns to arbitrary substrates with graphene or gelatin" springer, pp. 115-119, 2023.

[37] M. J. Bethea, R. Singh, H. Mirza Jani, E. Istif, M. J. Akhtar, T. Abbas, "Photolithography-Based Microfabrication of Biodegradable Flexible and Stretchable Sensors", Advanced material. Vol. 35, Issue. 6, pp. 311-315, February 9, 2023.

[38] H. Kim, Kwang, J. Kim, Doh-Soon Kwak, "A case study on modelling and optimizing photolithography stage of semiconductor fabrication process" Kim Quality and Reliability Engineering International - Wiley Online Library, vol. 26, Issue 7, pp. 764-775, 2010.

[39] X. Wang, S. Guo, Y. Tong, X. Zhao, Q. Tang, Y. Liu, "Photolithographic transparent flexible graphene oxide/ PEDOT: PSS electrode array for conformal organic transistor". IEEE Electron Device Lett. 43, 2109–2112 (2022).

[40] Rajiv Kohli and K.L. Mittal, "Methods for Assessment and Verification of Cleanliness of Surfaces and Characterization of Surface Contaminants", Vol. 12, p.p.23-35, (2019).

[41] A. Choi, A. Hoang, T. Van Ngoc, "Residue-free photolithographic patterning of graphene". Chemical Engineering Journal. Vol. 429, pp. 412-416, (2022).

[42] H. Lee, C. yun, S. Cho. "A simple fabrication method of passive-matrix organic light-emitting diode display without a photolithography process". Solid-State Electronics. Volume 208, pp. 1206-1209, October 2023.

[43] X. Wang, Cheng "Defect-related properties of optical coatings". Advanced Optical Technologies. De Gruyter, Volume 3 Issue 1,pp 243-252, February 1, 2014.

[44] W. Lee, J.T. Robinson, K.E. Whitener, "Graphene-enabled block copolymer lithography transfer to arbitrary substrates". Nano Express, Volume 2, Number 1, pp. 97-101, (2021).

[45] T. Sekiguchi, H. Ueno, "UV-curable Polydimethylsiloxane Photolithography and Its Application to Flexible Mechanical Metamaterials", Sensors and Materials, Vol. 35, No. 6, pp. 1098-1104, (2023).

[46] FPD Lithography Equipment | Canon Global .

الخلاصة

تبحث هذه الأطروحة في طريقة تصميم وتقييم أجهزة التصنيع الدقيق للإلكترونيات منخفضة التكلفة على ركائز منفصلة (زجاج، سيليكون، (Al، Cu) كوسيلة لتطوير أغشية رقيقة من النحاس والألومنيوم بلاستيك). سمك الفيلم، يتم أيضًا استكشاف طرق سمك الحوسبة والنظر فيها. مناقشة كاملة لتصميم وتشغيل جهاز التفريغ المستخدم في تصنيع أفلام النحاس والألومنيوم. تم تقديم التطور بالإضافة إلى التحسين التالي في دراسة البلورات ودراسة مورفولوجية القوى (AFM) الذي يمكن إجراؤه. تم استخدام مجهر القوة الذرية الذرية المجهرية. ويظهر زيادة الخشونة مع زيادة السماكة. الغرض من تبخير أكثر من مادة والفحص بمجهر القوة الذرية لأكثر من مادة وعلى أكثر من ركيزة هو التأكد من كفاءة الجهاز في ترسيب الأغشية الرقيقة ومعرفة التيارات العالية المطلوبة ومعرفة تعرف على ضغوط الفراغ العالية. لا يحدث أي ترسيب عندما يكون التيار أقل من 115 أ. لا يحدث أي ترسيب عندما يكون وقت الترسيب أقل من 30 دقيقة. ومن خلال النتائج التي تم الحصول عليها ومن خلال المقارنات التي تم إجراؤها مع الأجهزة الأخرى، فإن الجهاز المستخدم يعطي نتائج مماثلة مع تيار أعلى، وضغط أقل، ونظام تبريد أقل تعقيدا، ووحدة إمداد طاقة أكبر. تركز هذه الدراسة أيضًا على تحسين خطوة الطباعة الحجرية الضوئية لزيادة المحاذاة وتنفيذ الأبعاد الحرجة، وهي معلمة جودة لأجهزة أشباه الموصلات. وقد وجد أن الأداء المتوقع للخيار الأمثل قريب من الحد المتوقع للتحسين في النموذج. يتم تطبيق طبقة مقاومة للضوء على المادة المراد نقشها. اعتمادًا على ما إذا كانت مقاومة الضوء المستخدمة إيجابية أم سلبية، تمت إزالة مكونات مقاومة الضوء المكشوفة أو غير المكشوفة أثناء عملية تطوير المقاومة. يتم إنشاء تصميم القناع، ويمكنه إنتاج تصميمات أقنعة مختلفة على نطاق صغير الناتج كفيلم إيجابي. في هذه التجربة، تم PDF تتم طباعة تصميم قناع ملف .AutoCAD بواسطة برنامج استخدام طبقة زجاجية موحدة كركيزة بطول 2.5 سم وعرض 2.5 سم وسمك 0.2 سم. تؤثر عناصر .مختلفة، مثل التلوث والالتصاق ومعدل التعرض والحساسية ومصدر التعرض، على أداء مقاوم الضوء

جمهورية العراق
وزارة التعليم العالي والبحث العلمي
جامعة بابل
كلية الهندسة
قسم الهندسة الكهربائية

بناء نظام لتصنيع الالكترونيات واطئ الكلفة

رسالة

مقدمة الى كلية الهندسة / جامعة بابل

كجزء من متطلبات نيل درجة الماجستير في الهندسة الكهربائية / إلكترونيك

من قبل

احمد محسن ناصر حسين

اشراف

د. حيدر صاحب منجي المؤمن

1445هـ 2023م